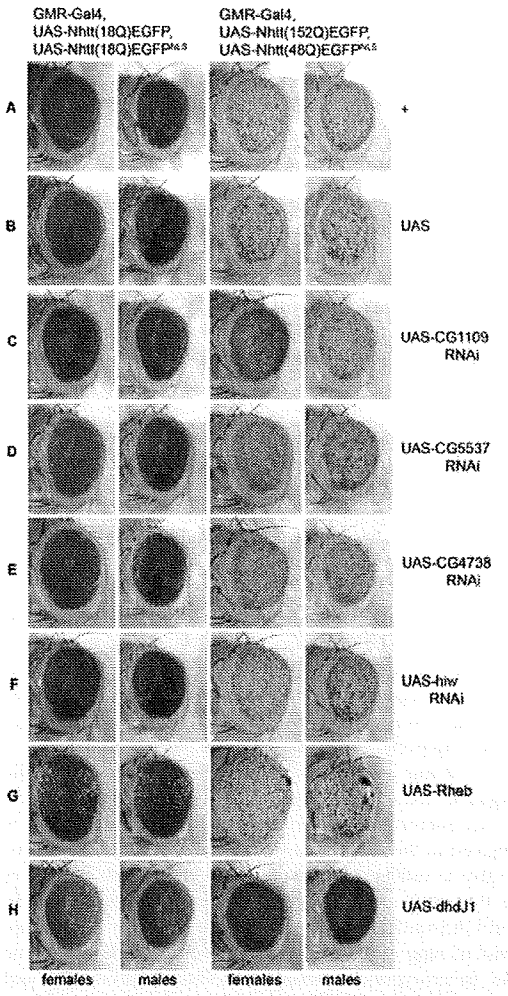

Figure 4. Selected screen candidates modify mutant Htt-induced toxicity in the fly eye. GMR-Gal4-driven expression of UAS-Nhtt(152Q)EGFP, UAS-Nhtt(48Q)^{NLS} in the compound eye results in a progressive loss of pigmentation compared to expression of UAS-Nhtt(18Q)EGFP, UAS-Nhtt(18Q)^{NLS} (**A**). Carrying an extra UAS transgene does not noticeably alter this phenotype (**B**). Female flies carrying a UAS-CG1109 RNAi transgene on the X chromosome show a clear suppression of the mutant Htt-induced toxicity phenotype, whereas no clear modification is seen in male flies lacking the UAS-CG1109 RNAi transgene (**C**). Expression of UAS-CG5537 RNAi on the X chromsome (**D**), and an autosomal UAS-CG4738 RNAi transgene (**E**) also suppress the mutant Htt-induced degenerative phenotype, with a rescue of pigmentation in these flies. Note: both males and females carry a copy of the for the UAS-CG5537 RNAi transgene as explained in Materials and Methods. Flies carrying a UAS-hiw RNAi transgene showed a slight rough eye phenotype that was also observed when coexpressed with normal Htt (**F**). Overexpression of Rheb resulted in a drastic enhancement of the Htt phenotype with an increase in black necrotic patches, further loss of pigmentation and a rough eye with bristle disorganization (**G**). Overexpression of Rheb in flies expressing normal Htt also resulted in a rough eye phenotype with a mild loss of pigmentation. The chaperone molecule, dhdJ1 clearly suppressed Htt-induced loss of pigmentation when overexpressed (**H**). All flies were aged between 21 and 22 days.
doi:10.1371/journal.pone.0007275.g004

consistent results with this candidate. However, a slight rough eye with disruption to eye bristles was observed in a mutant Htt-independent manner (Figure 4F). Overexpression of Rheb enhanced the phenotype of mutant Htt flies, with a severe rough eye phenotype and enhancement of pigment cell loss (Figure 4G right panels). However, overexpression of Rheb in flies expressing our NhttEGFP transgene with a normal length polyQ repeat (Figure 4G left panels) or expression of UAS-Rheb alone (data not shown) also resulted in a rough eye phenotype with bristle disorganization. As a control, we used the overexpression of the *Drosophila* homologue of heat shock protein 40, dhdJ1, to suppress the mutant Htt eye phenotype (Figure 4H).

Validation of RNAi screen candidates in aged adult fly brain

We further confirmed the validity of CG5537 and CG4738 RNAi by quantification of mutant Nhtt(98Q)EGFP brain aggregates. 4 week old male brains, from Elav-Gal4, UAS-Nhtt(98Q)EGFP recombinant lines were dissected and stained with anti-elav antibody and Hoechst 33345. We quantified the number and size of brain aggregates from stacked images of 5 μm confocal sections, using ImageJ software. We observed a significant decrease in the average number of visible inclusions in each brain by expression of UAS-CG4738 RNAi and UAS-CG5537 RNAi (Figure 5B and 5C). Although Rheb overexpression did not significantly increase the number of brain inclusions or the inclusion load, the average aggregate size was increased (Figure 5C).

In summary, by using various *in vivo* models of HD we have validated the effect of several candidate genes identified through a large-scale RNAi screen for modifiers of mutant Htt aggregation.

Discussion

To make use of the amenability of cultured *Drosophila* cells to gene knockdown by RNAi, we aimed to screen a library of dsRNA molecules covering around half of the fly genome and enriched for fly genes with mammalian homologues, for modifiers of Htt(62Q)EGFP aggregation. We carried out several rounds of screening to identify such modifier dsRNAs and carefully confirmed our screen results by addressing issues such as non-specific transcript reduction and potential gene off-targeting. Following our stringent screening method, our final 3 groups of candidates were assessed biochemically by Western Blot analysis and visually by confocal microscopy.

Our candidates fell into several functional groups, the most notable being transport molecules, including those involved in nuclear transport, and nucleotide processing including RNA metabolism. Nuclear transport has been reported to be important in mutant Htt pathogenesis, with Htt itself reportedly shuttling between the nucleus and the cytoplasm [10,13]. RNA metabolic processes are receiving increasing attention in the neurodegenerative field and RNA binding proteins have been identified as polyglutamine aggregate-interacting proteins and contributing to polyglutamine disease pathogenesis [14,15]. Although we identified many genes through RNAi screening with predicted involvement in the Ubiquitin Proteasome System (UPS), most were aggregation-suppressing. This may be due to the essential role of many of these genes, most of which were eliminated by OTE pruning and secondary screening for reduction of Nhtt(18Q)EGFP, although we cannot exclude the possibility that some eliminated dsRNAs might reduce Nhtt(18Q)EGFP expression by enhancing cellular proteolytic activities. Loss of the ubiquitin ligase highwire consistently resulted in an increase in

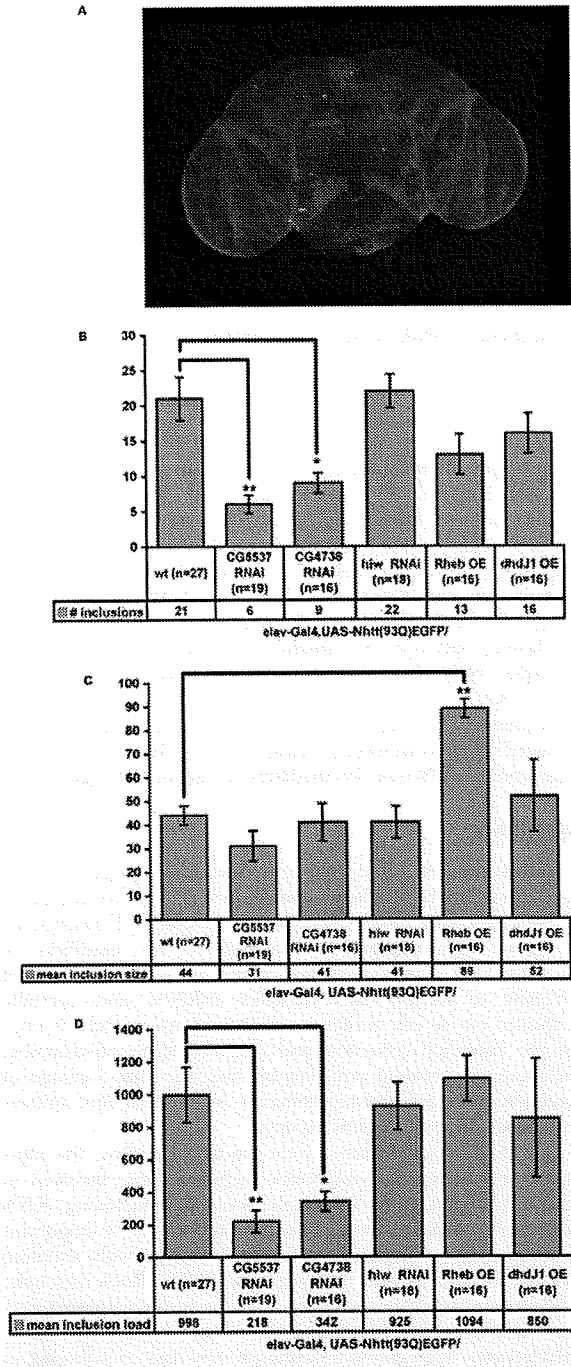

Figure 5. CG5537 and CG4738 RNAi transgenese suppress Htt(93Q)EGFP aggregation in aged *Drosophila* brain. 4-week old (28–29 days) fly brains were dissected from male flies and stained with α-elav antibody (magenta), imaged by confocal microscopy and 5 μm z stacks projected into one image (**A**). Compared to elav-Gal4, UAS-Nhtt(93Q)EGFP/wt flies, flies carrying a UAS-CG5537 RNAi or UAS-CG4738 RNAi transgene show a significant reduction in the mean number of inclusions (**B**) and the mean overall inclusion load (# inclusions X mean inclusion size) (**D**) with no significant reduction in inclusion size observed (**C**). UAS-hiw RNAi and UAS-dhdJ1 had no significant effect on the number, size or load of inclusions (**B–D** respectively). UAS-Rheb significantly increased the mean inclusion size (**C**), however there was an insignificant reduction in inclusion number (**A**) with no significant change in overall inclusion load (**D**). Error bars represent +/− SEM. The total number of brains imaged and scored from 1 to 3 experiments are indicated in the data box. ** $p \leq 0.0008$, * $p \leq 0.008$, Student's t test.
doi:10.1371/journal.pone.0007275.g005

mutant Htt inclusion number and size in our cell culture model of HD and appeared to enhance the eye degeneration phenotype of mutant Htt, although the high degree of phenotypic variability with the UAS-hiw RNAi lines used made it difficult to reach a sure conclusion on the role of this gene in HD pathogenesis. Furthermore, no significant difference was found in the number or size of inclusions in aged adult brains expressing UAS-hiw RNAi (Figure 5).

Our screen was biased towards detecting suppressors due to the high aggregation propensity of our cell line. Investigation of aggregation-enhancing dsRNAs with z scores slightly below our +2SD cut-off (z scores between 1.5 and 2) revealed several UPS dsRNAs of the ubiquitin-ligase class. This is consistent with the role played by the UPS system in targeting mutant Htt for degradation. This group of enhancers can be viewed as an excel spreadsheet in Data S1.

To further validate our high-confidence candidates, we established *in vivo* models of HD to investigate whether or not these genes are likely to be involved in mutant Htt toxicity and/or modification of mutant Htt aggregation *in vivo*. The *Drosophila* compound eye has long been utilized to assess potential genetic interactions particularly in the fields of apoptosis and degeneration in part because the eye is sensitive to cell loss and produces a visible phenotype when the highly organized ommatidial structure is disrupted. Furthermore, the eye is not essential for viability, allowing genetic interactions to be investigated in the adult, even with highly toxic gene products. We were able to validate the role of several of our gene candidates using the fly eye as a model system. Expression of UAS-CG4738 RNAi and UAS-CG5537 RNAi transgenes resulted in a noticeable and consistent suppression of the loss of pigmentation phenotype caused by heterozygous expression of Nhtt(48Q)EGFP^{NLS} and Nhtt(152Q)EGFP (Figure 4). We also observed a strong suppression of this phenotype with UAS-CG1109 RNAi and a strong enhancement of the phenotype by overexpression of Rheb, consistent with the role of autophagy in Htt aggregation [16,17].

Limiting our *in vivo* validation of candidates to the eye raised several problems. Although the eye is valuable as a toxicity model, the relationship between polyglutamine aggregation and toxicity is not clear in the eye. Overexpression of the heat shock protein 40 homologue, dhdJ1, demonstrates a drastic suppression of ataxin 1-induced toxicity [18] and in our hands, this same transgene resulted in suppression of mutant Htt-induced toxicity. However, suppression of polyglutamine toxicity was independent of a visible change in ataxin-1 aggregation [18]. We therefore set out to assess the role of selected candidates in aggregation of mutant Htt in aged adult fly brain. Our aggregation model, expressing one copy of a UAS-Nhtt(93Q)EGFP transgene using the pan-neuronal driver, elav-Gal4, formed visible inclusions in the brain and optic lobes (Figure 5A). Although all progeny differed in age by no more than 24 hours, there was a high degree of variation in the number and size of visible inclusions. Nevertheless, we found a significant reduction in the number of inclusions and overall inclusion load by expression of UAS-CG4738 RNAi and UAS-CG5537 RNAi. We could not obtain a clear brain aggregation result for CG1109 due to poor brain quality for all progeny from this cross. CG1109 is a novel gene, recently identified in a primary neuronal RNAi screen

for genes required for neurogenesis [19]. CG1109 may therefore be essential for neuron function and pan-neuronal expression of an RNAi construct may be toxic.

We were unable to detect a significant reduction in mutant Htt inclusions in the brain by overexpression of dhdJ1. It is possible that dhdJ1 requires some cofactor for its function as a heat shock protein that may be lacking in elav-positive neurons in the fly brain. However, given that so many studies use the eye for validation of polyglutamine modifiers, it should be noted that perhaps not all such modifiers will prove valid in models for mutant Htt aggregation. Our strongest candidates, CG4738 and CG5537 were validated by two independent RNAi stocks in the eye model (Figure 4 and data not shown).

Although some corresponding results were observed between suppressor activity in the cellular system and reducing toxicity in eye, the discrepancy is not unexpected. Even in our cellular system, based on the inclusion formation and cell viability, a distinct correlation was not confirmed (Table 1, Figure S7). Previously, drugs have been screened for their effect on polyglutamine aggregate formation using cellular models. One drug inhibited aggregation and suppressed neurodegeration [20,21]. Another compound was reported to promote inclusion formation and prevent the huntingtin-mediated proteasome dysfunction, which is related to cell toxicity [22,23]. These results and the existence of heterogeneous aggregate species such as fibrils and oligomers suggest that the decrease of inclusions might correlate to the change of some specific toxic species of aggregates depending on the system used.

We further examined the functional relationship among mouse homologues of the selected candidates (Figure S8). The main gene group includes nucleotide processing, nucleoporin and signaling. The signaling genes are related to the autophagy system, which could degrade polyglutamine aggregates. The role of other major groups on aggregate formation, such as genes for nucleotide processing and nucleoporin, is unknown. Since the main localization of these gene products is nucleus, their function may be related to the formation of nuclear inclusions. Reduction of the nucleoporin 160 protein (CG4738) consistently rescued Htt-induced toxicity and aggregation in our cell line and *in vivo*. It is feasible, however, that a nucleoporin may act as a docking site for the accumulation and aggregation of mutant Htt. Further work remains to elucidate the role of our candidates in the mammalian system and their mechanism of action.

In summary, we have carried out a thorough screen for modifiers of mutant human Htt aggregation using new models of HD established in cultured *Drosophila* cells and in the fly. Further investigation of our candidates, particularly those involved in nucleotide processesing and intracellular transport, including nuclear transport may uncover, as yet, unexplored pathways relevant to human Huntington Disease pathogenesis.

Methods

Cloning of *Drosophila* constructs

We cloned N-terminal Htt exon 1 with 18Q, 62Q or 152Q as fusions with EGFP and containing a C terminal NLS and MYC tag into *Drosophila* expression vectors as described in Supporting Information.

Establishment of stable, inducible *Drosophila* cells expressing Htt exon 1-EGFP

We established stable, single colony-isolated BG2 cell lines using the DES® system (Invitrogen) as per the manufacturer's instructions. Briefly, larval central nervous system-derived parental cells, BG2-c2 cells [24] were cotransfected with copper-inducible pRMHa3-NhttEGFP encoding either an 18Q or a 62Q repeat together with pCoBlast to confer Blasticidin-resistance. Stably-integrated heterogeneous cells were selected in the presence of 25 ug/ml Blasticidin. 1–3 cells were seeded into 96 well plates and isolated colonies were picked and expanded. Individual clones were checked for expression of the NhttEGFP transgene by microscopy and Western blot analysis following induction with $CuSO_4$. Cells were cultured in Schneider's *Drosophila* Medium (Invitrogen) supplemented with 10% heat-inactivated FBS (Sigma) and 10 µg/ml insulin (Sigma). Medium was supplemented with 0.5 mM $CuSO_4$ for induction of NhttEGFP expression. Following initial selection, HD cell lines were not maintained in Blasticidin.

dsRNA library synthesis

In vitro transcription reactions were set up in 96 well U-bottom plates (Cellstar) using Ambion T7 megascript kits to simultaneously synthesize sense and antisense RNA strands in one reaction and purified as described in Text S1.

ArrayScan® analysis

Fixed, stained cells were analyzed by ArrayScan®V^{TI} High Content Screening (HSC) Reader (Cellomics, Pittsburgh, PA, USA) using Target Activation Bio Application (TABa). TABa analyzes images acquired by an HSC Reader and provides measurements of the intracellular fluorescence intensity and localization on a cell-by-cell basis.

In each well, several thousand cells were counted and quantified for the number and size of Nhtt(62)EGFP inclusions. Nuclei stained by Hoechst 33285 provided the autofocus target and scored the number of quantified cells. Screening consisted of two scans using Hoechst and FITC (for EGFP) fluorescence. At first, the number of aggregates was calculated. Fluorescent spots of at least 5 pixels in size (magnification 40×) with an average EGFP intensity of more than 1500 were labeled as inclusions. Secondly, nuclei were defined as the objects of interest and their number was determined. EGFP intensity in each cell was calculated in the perinuclear region within the distance of 3 pixels from the nucleus and when the average intensity exceeded 250, the cell was considered as EGFP-positive. The percentage of the cells with aggregates was calculated.

ArrayScan® data was used to calculate the number of inclusions per cell (inclusion #/cell) and the inclusion load per cell (inclusion load/cell), which takes into account the inclusion size (inclusion number multiplied by inclusion size and divided by the total number of cells).

Large scale RNAi screening

Detailed methods of our large-scale RNAi screen including methodology can be found in Text S1.

Fly stocks

NhttEGFP transgenes with either an 18Q or 152Q polyglutamine repeat and either with or without a nuclear localization signal (NLS) were subcloned into pUAST plasmid and injected by standard methods into w^{1118} embryos to establish transgenic flies. Driver lines used in our analysis were obtained from the Bloomington stock centre and were recombined with our transgene(s) for stable expression. Due to CAG repeat instability, some fly stocks were injected with constructs with repeat lengths other than 152Q. In such cases, where expressed protein sizes assessed by Western blotting were inconsistent with a 152Q repeat, the transgene was amplified by RT-PCR and the CAG repeat sequenced. UAS-dhdJ1 have been previously described and were

kindly provided by Prof. Kazemi-Esfarjani [18]. RNAi flies were obtained from the VDRC stock centre [12] in Vienna and the NIG stock centre in Mishima. UAS-Rheb flies and the GMR-Gal4 and elav-Gal4 driver lines were obtained from the Bloomington stock centre. For all autosomal insertion lines and UAS-CG1109 RNAi, we set up crosses with virgin females carrying our Htt transgenes to males carrying the candidate transgene. For crosses with UAS-CG5537 RNAi, virgin females were crossed to HD males.

Prediction of Off-Target Effects

The amplicon sequence for each dsRNA in the Open Biosystems library was automatically retrieved from the FLIGHT database and entered into the *Drosophila* Resource Screening Center (DRSC) OTE search tool to predict the number of potential Off-Target Effects with a 19 nt match.

De novo design of amplicons for RNAi

The transcript sequences for the final candidates were retrieved from FlyBase and the region targeted by the Open Biosystems dsRNA was manually highlighted. Transcript sequence not targeted by the library was used to design T7-tagged oligos for amplication of *de novo* RNAi probes using the E-RNAi tool (Heidlberg, Germany). Where possible, probes were selected to target all possible transcripts of a given gene and had no predicted 21 nt OTEs.

Synthesis of *de novo* RNAi probes

To prepare the template for PCR amplification of the target regions for *in vitro* transcription (IVT), total RNA was prepared from 200 liquid N_2 freeze-dried whole w^{1118} flies using TRIzol® reagent (Invitrogen). Oligo d(T)-primed cDNA was synthesized from 2 µg total RNA, using First Strand cDNA synthesis kit according to the Manufacturer's directions (Novagen). 3 µl were used in a standard PCR reaction using KODPlus DNA polymerase (TOYOBO, Japan) and using the primer pairs designed as described above and synthesized by Operon. PCR products were purified using the Vacuum Manifold® system (Millipore) and a sample was checked by agarose gel electroporesis. Purified PCR products containing T7 promoters at each end were used as templates for *in vitro* transcription using the Megascript T7 kit (Ambion) according to the manufacturer's directions. dsRNA is automatically made as each strand is synthesized in a single reaction. dsRNAs were purified using the Millipore Vacuum Manifold system and the concentration calculated by spectrophotometry. In cases where multiple bands were observed in the PCR product, the band of the correct size was excised and purified using the Wizard® Gel and PCR Clean-Up kit (Promega) before being used as a template for IVT.

Tertiary Screening using *de novo* dsRNAs

Based on calculations of Clemens *et al*, 2000 we brought each dsRNA to 860 nM stock and aliquoted the appropriate amounts for 43 nM and 108 nM treatments into 96 well plates. Cells were treated with each *de novo* dsRNA probe in duplicate on separate experimental days and in different well positions. Each plate was arrayed with controls against NewLacZ, diap1 and dhdJ1 (hsp40). Scores were normalized by dividing the inclusions/cell value by the NewLacZ control value. Averaged, normalized scores for # inclusions/cell and inclusion load/cell were calculated.

Western Blot analysis

BG2-Nhtt(62Q)EGFP cells were treated with 43 nM dsRNAs for 48 hours in 12 well plates and the culture medium was replaced with induction medium containing 0.5 mM $CuSO_4$ for 16 hours. Cells were washed in PBS and then harvested in 1% SDS/PBS supplemented with Complete® Protease Inhibitor Cocktail (Roche), and divided into two for WB analysis and prepareation of total RNA. Cells for WB analysis were lysed by sonication, gently centrifuged and the protein concentration measured by BCA assay. 3 µg of whole cell lysates were boiled in LDS sample buffer/DTT and electrophoresed at 200 V through a 4–12% NuPAGE gel (Invitrogen) in MOPS buffer. Proteins were transferred wet onto PVDF (Millipore) membrane, blocked in 10% skim milk and blotted with EM48 MAB5374 Huntingtin primary antibody (Millipore) and Mouse IgG Peroxidase (GE healthcare) secondary antibody before detection using ECL. Images were captured using LAS-1000 (Fujifilm). Blots were stripped and re-probed with E7 β-tubulin antibody (Hybridoma Bank) and Mouse IgG Peroxidase (GE). The presence of aggregates in whole cell lysates makes quantification difficult, resulting in some apparent loading differences between samples.

Imaging of adult fly eyes

Fly progeny were collected every 24 hours over a 5 day period and aged for 3 weeks (21–22 days). Flies were randomly selected, anesthetized with CO_2 and decapitated. Fly heads were aligned on a slide for imaging the left eye and viewed using an Olympus SZX16 dissecting microscope and an external light source (Kenko). Images were captured using a NIKON digital sight DS-L1 camera.

In vivo scoring of aggregation

For quantification of inclusions in the adult brain, brains from male flies aged for 4 weeks (28–29 days) were dissected in PBS and immediately fixed in 4% PFA for 30–60 minutes. Brains were fixed in paraformaldehyde and stained with elav antibody (Developmental Hybridoma Bank, Iowa, USA). Using a 10X objective lens, 5 µm z sections were imaged using a SP2nLeica Confocal and images were converted to greyscale JPEG images using Photoshop and then opened in ImageJ [25] for quantification of aggregation. In some cases, highly fluorescent areas clearly not inclusions, were removed to avoid artificial inclusion counts. The number and size of Htt(93Q)EGFP inclusions were quantified using ImageJ software on greyscale brain images captured by confocal microscopy using the green channel only. Threshold settings were set to a minimum of 100 and the default maximum (255). Using the 'Analyze Particles' option, the inclusion number and average inclusion size were calculated. We were unable to confirm expression levels of our candidates in adult brain by RTPCR, probably because contribution of non-RNAi targeted cell types contributing to the total RNA prepared could mask any reduction in elav-positive cells. We were able to detect the overexpression of dhdJ1 and Rheb in the eye model, suggesting that these transgenes are effectively overexpressing these genes (data not shown).

Supporting Information

Text S1 Supporting Materials and Methods
Found at: doi:10.1371/journal.pone.0007275.s001 (0.03 MB DOC)

Figure S1 RNAi screening validation and overview. The efficacy of RNAi treatment in a Drosophila cell culture model of HD was tested using dsRNA against GFP. Cells expressing BG2-Nhtt(18Q)EGFP cells treated with 37 nM GFP dsRNA for 48 hours and visualized by fluorescence microscopy show ablation of GFP (A). BG2-Nhtt(62Q)EGFP cells were treated with GFP

dsRNA and analyzed by ArrayScan®. Reduction of Nhtt(62Q)EGFP by GFP dsRNA reduced the number of EGFP-positive cells (B) and the number of EGFP-positive intracellular inclusions (C) detected by ArrayScan®. Screening in 96 well plate format was validated using a screen plate arrayed with random dsRNAs including dsRNA against diap1. Loss of diap1 results in widespread apoptosis as shown by the reduced viability in cells treated with diap1 dsRNA (D). An overview of our approach to screening for modifiers of mutant Htt aggregation, including several rounds of screening in vitro, followed by validation in vivo, is shown (E).
Found at: doi:10.1371/journal.pone.0007275.s002 (2.33 MB TIF)

Figure S2 OTE pruning following primary screening. Top pie charts show the functional categorization of all candidates following primary screening in BG2-Nhtt(62)EGFP cells. These candidates were pruned to eliminated dsRNAs with more than 10 predicted OTEs. The Specific Transcription category, including many transcription factors (TFs) was the most drastically reduced following OTE pruning, consistent with the fact that many TFs have repetitive trinucleotide repeats that are sensitive to off-targeting.
Found at: doi:10.1371/journal.pone.0007275.s003 (1.81 MB TIF)

Figure S3 Off-target effects reduce cell viability and contribute to false positive candidates. The mean cell viability values for candidates following primary screening were plotted against the number of predicted 19 nt OTEs, demonstrating a significant negative correlation between cell viability and the number of potential OTEs (A). dsRNAs with multiple predicted OTEs are over-represented amongst our candidates following the primary screen. 54% of the dsRNA target sequences in the Open Biosystems library have no predicted 19 nt OTEs, with only 5.7% having more than 10 predicted OTEs (B). In contrast, 30% of our candidates lacked any predicted OTEs, with 44% having greater than 10 potential off-targets (C). The presence of off-target sequences causes inconsistencies in assay results. The percentage of candidates that modified Nhtt(62Q)EGFP consistently from the primary screen, using library dsRNAs, and the tertiary screen, using de novo designed dsRNAs are shown in yellow. The percentage of candidates producing an opposite effect is shown in green, while pink shows the percentage of candidates that gave inconsistent results within the tertiary screen duplicates using de novo dsRNAs with no 21 nt OTEs. The majority of candidates with no more than 1 OTE consistently modified mutant Htt aggregation in vitro. Increasing OTEs increased the likelihood of inconsistent results (D).
Found at: doi:10.1371/journal.pone.0007275.s004 (2.19 MB TIF)

Figure S4 de novo RNAi probes. Target sequences were amplified with primers harboring the T7 promoter sequence. PCR products were purified using the Millipore Vacuum manifold system and checked for size and product specificity by agarose gel electrophoresis (top panel). In cases where more than one product was amplified, the product of the correct size was excised from the gel and purified. These products were then checked again by agarose gel electrophoresis (top right panel). To confirm the integrity of dsRNA synthesized in vitro from the PCR product templates, we ran 1 μg dsRNA on a denaturing formaldehyde gel (lower panel). Predominant bands are consistent with the predicted size for denatured RNA. We suspect the minor slower-migrating bands are non-denatured dsRNAs (A). By using RTPCR in BG2-Nhtt(62Q)EGFP cells treated with candidate groups 1–3 dsRNAs, we confirmed that in each case, the target gene was reduced upon dsRNA treatment. All results were from the same experiment except ATPsyn-b (boxed), which was from a different experiment (B).
Found at: doi:10.1371/journal.pone.0007275.s005 (1.59 MB TIF)

Figure S5 Confocal microscopy of RNAi-treated cells. BG2-Nhtt(62Q)EGFP cells treated with candidate groups 1–3 aggregation-suppressing (A) and aggregation-enhancing (B) dsRNAs. To demonstrate the increase in diffuse-expressing cells among aggregation-suppressors, the EGFP gain was increased to 400 compared with a gain setting of 300 for imaging the aggregation-enhancing dsRNAs.
Found at: doi:10.1371/journal.pone.0007275.s006 (6.00 MB TIF)

Figure S6 Confocal projection images of 3rd instar larval eye imaginal discs. Wandering 3rd instar larval eye discs were dissected in PBS, fixed in 4% PFA, stained with Hoechst and mounted onto a microscope slide in 80% glycerol for imaging using a Leica SP2 confocal microscope. Flies expressing Nhtt(18Q)EGFP together with Nhtt(18Q)EGFPNLS show localization of the protein in the nucleus (white arrow heads) and in the cytoplasm (white arrows) (left panels). Flies expressing mutant Nhtt(152Q)EGFP together with Nhtt(48Q)EGFPNLS show the presence of EGFP-positive nuclear (arrow heads) and cytoplasmic (white arrows) inclusions in larval eye imaginal discs (right panels). Images represent projection stacks of 5 μm z sections.
Found at: doi:10.1371/journal.pone.0007275.s007 (2.47 MB TIF)

Figure S7 Correlation between inclusion number/load and cell viability. Based on the data shown in Table 1, the values of % viability were plotted against those of fold change in the number of inclusions or inclusion load for all candidate genes. A weak positive correlation was observed between cell viability and both number of inclusions ($r = 0.436$, $P = 0.048$) and inclusion load ($r = 0.444$, $P = 0.044$).
Found at: doi:10.1371/journal.pone.0007275.s008 (2.46 MB TIF)

Figure S8 Functional grouping of mammalian orthologues of the candidate genes. The mammalian orthologues of the candidate genes (Table 1) identified by RNAi screening were categorized according to their known or predicted functions manually retrieved from the public databases such as PUBMED, Entrez Gene, and HomoloGene. Mammalian orthologues of enhancers and suppressors dsRNAs in the fly are shown by red- and blue-colored circles, respectively.
Found at: doi:10.1371/journal.pone.0007275.s009 (3.79 MB TIF)

Data S1 Excel file: Full List Functional Assign Worksheet: 2SDs full list All candidates with z scores of greater than 2 or less than −2 are shown in this worksheet, with data for Gene Ontology categorization and manual functional grouping. The effect on mutant Htt aggregation is abbreviated as either enhancing aggregation (en) or suppressing aggregation (su). The predicted number of 19 nt OTEs and the mean % viability values are shown. Given the continual updating of public databases, current information may differ from information obtained at the time this spreadsheet was made. Worksheet: en 1.5 to 2 Weaker enhancer dsRNAs with z scores between 1.5 and 2 are shown with all the data entries as above.
Found at: doi:10.1371/journal.pone.0007275.s010 (0.51 MB XLS)

Acknowledgments

We thank Ritsuko Kazama for synthesis of the dsRNA from library templates and to Dr. Peter Bauer for assistance with ArrayScan® operation. We are grateful to Prof. Masayuki Miura and Assoc. Prof. Erina Kuranaga for helpful discussions regarding the project design and *in vivo* methodology.

We thank the Bloomington, VDRC and NIG stock centers for provision of flies. UAS-dhdJ1 flies were a kind gift from Prof. Kazemi-Esfarjani.

Author Contributions

Conceived and designed the experiments: JD NN. Performed the experiments: JD KW. Analyzed the data: JD YK. Contributed reagents/materials/analysis tools: JD KW AWM. Wrote the paper: JD NN. Discussions and project supervision: NN. The design and implementation of the experiments including establishment of cell culture and in vivo models: JD. Carrying out the RNAi high-throughput screen, data analysis, cell treatments, microscopy, de novo probe design and all in vivo experiments: JD. Synthesis and purification of dsRNAs, Western blot analysis, and RTPCR: KW. Analysis the functional roles of selected candidates and other data: YK. Support of Fly maintenance materials and facilities: AWM.

References

1. Gil JM, Rego AC (2008) Mechanisms of neurodegeneration in Huntington's disease. Eur J Neurosci 27: 2803–2820.
2. Celotto AM, Palladino MJ (2005) Drosophila: a "model" model system to study neurodegeneration. Mol Interv 5: 292–303.
3. Sang TK, Jackson GR (2005) Drosophila models of neurodegenerative disease. NeuroRx 2: 438–446.
4. Bilen J, Bonini NM (2005) Drosophila as a model for human neurodegenerative disease. Annu Rev Genet 39: 153–171.
5. Marsh JL, Thompson LM (2004) Can flies help humans treat neurodegenerative diseases? Bioessays 26: 485–496.
6. Ramadan N, Flockhart I, Booker M, Perrimon N, Mathey-Prevot B (2007) Design and implementation of high-throughput RNAi screens in cultured Drosophila cells. Nat Protoc 2: 2245–2264.
7. Clemens JC, Worby CA, Simonson-Leff N, Muda M, Maehama T, et al. (2000) Use of double-stranded RNA interference in Drosophila cell lines to dissect signal transduction pathways. Proc Natl Acad Sci U S A 97: 6499–6503.
8. Kulkarni MM, Booker M, Silver SJ, Friedman A, Hong P, et al. (2006) Evidence of off-target effects associated with long dsRNAs in Drosophila melanogaster cell-based assays. Nat Methods 3: 833–838.
9. Ma Y, Creanga A, Lum L, Beachy PA (2006) Prevalence of off-target effects in Drosophila RNA interference screens. Nature 443: 359–363.
10. Atwal RS, Xia J, Pinchev D, Taylor J, Epand RM, et al. (2007) Huntingtin has a membrane association signal that can modulate huntingtin aggregation, nuclear entry and toxicity. Hum Mol Genet 16: 2600–2615.
11. Arziman Z, Horn T, Boutros M (2005) E-RNAi: a web application to design optimized RNAi constructs. Nucleic Acids Res 33: W582–588.
12. Dietzl G, Chen D, Schnorrer F, Su KC, Barinova Y, et al. (2007) A genome-wide transgenic RNAi library for conditional gene inactivation in Drosophila. Nature 448: 151–156.
13. Cornett J, Cao F, Wang CE, Ross CA, Bates GP, et al. (2005) Polyglutamine expansion of huntingtin impairs its nuclear export. Nat Genet 37: 198–204.
14. Murata T, Suzuki E, Ito S, Sawatsubashi S, Zhao Y, et al. (2008) RNA-binding protein hoip accelerates polyQ-induced neurodegeneration in Drosophila. Biosci Biotechnol Biochem 72: 2255–2261.
15. Doi H, Okamura K, Bauer PO, Furukawa Y, Shimizu H, et al. (2008) RNA-binding protein TLS is a major nuclear aggregate-interacting protein in huntingtin exon 1 with expanded polyglutamine-expressing cells. J Biol Chem 283: 6489–6500.
16. Ravikumar B, Vacher C, Berger Z, Davies JE, Luo S, et al. (2004) Inhibition of mTOR induces autophagy and reduces toxicity of polyglutamine expansions in fly and mouse models of Huntington disease. Nat Genet 36: 585–595.
17. Yamamoto A, Cremona ML, Rothman JE (2006) Autophagy-mediated clearance of huntingtin aggregates triggered by the insulin-signaling pathway. J Cell Biol 172: 719–731.
18. Kazemi-Esfarjani P, Benzer S (2000) Genetic suppression of polyglutamine toxicity in Drosophila. Science 287: 1837–1840.
19. Bai J, Binari R, Ni JQ, Vijayakanthan M, Li HS, et al. (2008) RNA interference screening in Drosophila primary cells for genes involved in muscle assembly and maintenance. Development 135: 1439–1449.
20. Zhang X, Smith DL, Meriin AB, Engemann S, Russel DE, et al. (2005) A potent small molecule inhibits polyglutamine aggregation in Huntington's disease neurons and suppresses neurodegeneration in vivo. Proc Natl Acad Sci U S A 102: 892–897.
21. Desai UA, Pallos J, Ma AA, Stockwell BR, Thompson LM, et al. (2006) Biologically active molecules that reduce polyglutamine aggregation and toxicity. Hum Mol Genet 15: 2114–2124.
22. Bodner RA, Outeiro TF, Altmann S, Maxwell MM, Cho SH, et al. (2006) Pharmacological promotion of inclusion formation: a therapeutic approach for Huntington's and Parkinson's diseases. Proc Natl Acad Sci U S A 103: 4246–4251.
23. Jana NR, Zemskov EA, Wang G, Nukina N (2001) Altered proteasomal function due to the expression of polyglutamine-expanded truncated N-terminal huntingtin induces apoptosis by caspase activation through mitochondrial cytochrome c release. Hum Mol Genet 10: 1049–1059.
24. Ui-Tei K, Nagano M, Sato S, Miyata Y (2000) Calmodulin-dependent and -independent apoptosis in cell of a Drosophila neuronal cell line. Apoptosis 5: 133–140.
25. Abramoff MD, Magelhaes PJ, Ram SJ (2004) Image processing with imageJ. Biophotonics Int 11: 36–42.

Supplemental Material can be found at:
http://www.jbc.org/content/suppl/2009/03/12/M809229200.DC1.html

THE JOURNAL OF BIOLOGICAL CHEMISTRY VOL. 284, NO. 19, pp. 13153–13164, May 8, 2009
© 2009 by The American Society for Biochemistry and Molecular Biology, Inc. Printed in the U.S.A.

Inhibition of Rho Kinases Enhances the Degradation of Mutant Huntingtin*[S]

Received for publication, December 9, 2008, and in revised form, March 10, 2009 Published, JBC Papers in Press, March 11, 2009, DOI 10.1074/jbc.M809229200

Peter O. Bauer[1], **Hon Kit Wong, Fumitaka Oyama, Anand Goswami, Misako Okuno, Yoshihiro Kino, Haruko Miyazaki, and Nobuyuki Nukina**[2]

From the Laboratory for Structural Neuropathology, RIKEN Brain Science Institute, 2-1 Hirosawa Wako-shi, Saitama 351-0198, Japan

Huntington disease (HD) is a fatal hereditary neurodegenerative disease caused by an expansion of the polyglutamine (polyQ) stretch in huntingtin (htt). Whereas the pathological significance of the expanded polyQ has been clearly established and a tremendous effort to develop therapeutic tools for HD has been exerted, there is yet no effective cure. Whereas many molecules able to reduce the polyQ accumulation and aggregation have been identified, including several Rho kinase (ROCK) inhibitors, it remains very important to determine the mechanism of action of the potential drugs. ROCK inhibitors, including Y-27632 were reported to decrease aggregation of htt and androgen receptor (AR) through ROCK1 and protein kinase C-related protein kinase-2 (PRK-2). A downstream effector of ROCK1, actin-binding factor profilin, was shown to inhibit the mutant htt aggregation but not AR by direct interaction. We found that the anti-aggregation effect of ROCK inhibitors was not limited to the mutant htt and AR and that Y-27632 was also able to reduce the aggregation of ataxin-3 and atrophin-1 with expanded polyQ. These results suggested that in addition to the mechanism reported for htt and AR, there might also be other common mediators involved in the reduced aggregation of different polyQ proteins. In this study, we show that Y-27632 not only reduced the mutant htt aggregation by enhancing its degradation, but surprisingly was able to activate the main cellular degradation pathways, proteasome, and macroautophagy. We also show that this unique effect was mediated by ROCK1 and ROCK2.

Huntington disease (HD)[3] is a dominantly transmitted neurodegenerative disorder involving the basal ganglia and cerebral cortex that typically strikes in midlife, where survival from onset to death averages 17–20 years. Its prevalence is around 5–10 cases per 100,000 worldwide, which makes it one of the most common inherited neurodegenerative disorders. The characteristic symptoms of HD are involuntary choreiform movements, cognitive impairment, mood disorders, and behavioral changes that are chronic and progressive over the course of the illness. The underlying gene defect was proved to be a CAG repeat encoding polyglutamine (polyQ) in exon 1 of a 348-kDa protein named huntingtin (htt) (1, 2). In the unaffected population, the number of CAG repeats varies from 6 to 34 while repeats of 36 or more define an HD allele. The variability of the pathological alleles is quite wide, ranging from 36 to 121 repeats, displaying an inverse correlation with onset age (3).

Endogenous wild-type htt was shown to be essential for the normal development and health of the individual, but its mutated form confers a toxic gain-of-function (4). In 1997, polyQ aggregates were reported in the brains of transgenic mice and in the postmortem brains from patients with HD in the form of nuclear inclusions (5, 6).

Several models have been proposed to explain the mechanism by which the mutant htt causes neuronal degeneration (7), for example impairment of transcription and gene expression (8–11), impairment of axonal transport and synaptic transmission (12–14), suppression of energy metabolism (15, 16), and induction of apoptosis (17). Although controversial, mutant htt has also been proposed to impair the ubiquitin proteasome system (UPS) (18–21). Despite enormous progress in elucidating the molecular pathology of HD, the prognosis for patients has improved little since the first description of this disease, thus no effective treatments for HD patients have been developed.

Rho-associated kinases (ROCKs) are Ser/Thr protein kinases, which were found to be downstream targets of the small GTPase RhoA GTPase (22–24). In the mammalian system, ROCKs consist of two isoforms. ROCK1 (ROKβ, p160ROCK) is located on chromosome 18 and encodes a 1,354-amino acid protein (22). ROCK2 (ROKα), is located on chromosome 12 and contains 1,388 amino acids (25).

The ROCKs are important regulators of cell growth, migration, and apoptosis via control of actin cytoskeletal assembly. They regulate cell contraction through serine-threonine phos-

* This work was supported in part by a Grant-in-Aid for Scientific Research on Priority Areas (Research on Pathomechanisms of Brain Disorders) from the Ministry of Education, Culture, Sport, Science, and Technology of Japan (17025044) and by a Grant-in-Aid for the Research on Measures for Intractable Diseases from the Ministry of Health, Welfare and Labor of Japan. This work was also supported in part by a grant from the JSPS (Japan Society for the Promotion of Science).

[S] The on-line version of this article (available at http://www.jbc.org) contains supplemental Figs. S1 and S2.

[1] A JSPS Postdoctoral Fellow.

[2] To whom correspondence should be addressed. Fax: 8148-462-4796; E-mail: nukina@brain.riken.jp.

[3] The abbreviations used are: HD, Huntington disease; polyQ, polyglutamine; htt, huntingtin; AR, androgen receptor; DRPLA, dentatorubropallidoluysian atrophy; tNhtt, truncated N-terminal huntingtin; ROCK, Rho kinase; EGFP, enhanced green fluorescent protein; NLS, nuclear localization signal; mRFP, monomeric red fluorescence protein; Ub-dsRED, ubiquitinated discosoma red fluorescent protein; PI, propidium iodide; 3MA, 3-methyladenine; MEF, mouse embryonic fibroblasts; dbcAMP, N^6,2′-*O*-dibutyryladenosine-3′,5′-cyclic monophosphate sodium salt; RT-PCR, reverse transcriptase PCR; ponA, ponasterone A; FTA, filter trap assay; PBS, phosphate-buffered saline; shRNA, short hairpin RNA; PGPH, peptidyl glutamyl peptide hydrolase; UPS, ubiquitin proteasome system; PEA, phosphatidylethanolamine; PRK-2, protein kinase C-related protein kinase-2; ANOVA, analysis of variance.

Downloaded from www.jbc.org at RIKEN LIB, on December 13, 2009

Supplemental Material can be found at:
http://www.jbc.org/content/suppl/2009/03/12/M809229200.DC1.html

phorylation of adducin, ezrin-radixin-moesin (ERM) proteins, LIM kinase, myosin light chain phosphatase (MLCP), and Na/H exchanger 1 (NHE-1) (25, 26). RhoA/ROCK was shown to regulate the intracellular localization and phosphorylation of phosphatase and tensin homolog (PTEN), and RhoA/ROCK-mediated phosphorylation of PTEN is required for the phospholipid phosphatase activity of PTEN that antagonizes PI3K-mediated Akt signaling (27).

The RhoA/ROCK pathway was also reported to be implicated in the $A\beta_{42}$ processing (28). Using APPswe-expressing Neuro2a mouse neuroblastoma cells, it was demonstrated that ROCK modulates shedding of sAPPα induced by statins. Constitutively active ROCK mutant attenuated sAPPα shedding from both untreated and statin-treated cells, whereas a ROCK mutant without kinase activity activated sAPPα shedding (29). Calorie restriction (CR)-induced SIRT1 expression promotes α-secretase activity, sAPPα generation, and diminishes Aβ generation by neurons from *Tg2576* mice and CHO cells expressing APPswe. This effect of SIRT1 appears to be dependent on ROCK1 (30). The inhibition of ROCK activation was reported to be also an efficacious approach for the treatment of acute ischemic stroke (31).

Blocking the RhoA/ROCK pathway has been shown to markedly inhibit the polyQ protein aggregation and decrease its toxicity in cellular and *Drosophila* model of HD (32). ROCK1 and protein kinase C-related protein kinase-2 (PRK-2) have been identified to be the mediators of aggregation inhibition by Y-27632 (33). Moreover, a downstream effector of ROCK1, actin-binding factor profilin, was reported to inhibit the mutant htt aggregation by direct interaction via its polyproline-binding domain (34). Unlike htt, the inhibition of the mutant androgen receptor (AR) aggregation by profilin was not mediated by direct interaction (34).

We tested the effect of Y-27632 on several proteins with expanded polyQ and it was able to efficiently reduce the aggregation of these proteins. In addition to htt and AR, the tested proteins included mutant full-length and truncated ataxin-3 and full-length atrophin-1 with expanded polyQ (Fig. 1). Therefore in this study we investigated whether there might be a common mechanism by which the chemical ROCK inhibition leads to the reduced polyQ aggregation. We found that enhanced degradation of expanded polyQ protein largely contributes to this effect. Surprisingly, both major degradation systems, UPS and macroautophagy (hereafter referred to as autophagy), appeared to be activated by ROCK inhibition, and involved in reducing the polyQ aggregation.

EXPERIMENTAL PROCEDURES

Materials—The ROCK inhibitors Y-27632, HA1077, and H89 were obtained from Sigma. H-1152, propidium iodide (PI), and the autophagy activator, rapamycin (35) were from Calbiochem. Fluorescent nucleic acid stain Hoechst 33258 was from Molecular Probes. MG-132 (Z-Leu-Leu-Leu-aldehyde) was from Wako Chemicals and 3-methyladenine (3MA) was from Sigma.

Mouse monoclonal antibody specific for N-terminal of huntingtin (EM48) and rat monoclonal anti-β-tubulin antibodies were from Chemicon. Anti-LC3, anti-GFP, and anti-RFP antibodies were from MBL and anti-ubiquitin antibody was from DAKO. Mouse monoclonal anti-ROCK1 and anti-ROCK2 antibodies were purchased from BD Transduction Laboratories and anti-ATG5 antibody was kindly provided by Dr. Mizushima. All other chemicals were from Sigma or Nacalai tesque unless otherwise specified.

Plasmids—Plasmids encoding the truncated N-terminal of human huntingtin (tNhtt) with 16, 60, and 150 glutamine repeats were introduced in pEGFP-N1 vector as previously described (36). The construction of plasmids encoding human truncated or full-length ataxin-3 containing 130Q (in pEGFP-N1 vector) was described previously (37). Human androgen receptor with 23Q (AR23Q) was amplified from human brain cDNA library by PCR using a set of primers BglII-AR-Fw (5′-AAAAGATCTATGGAAGTGCAGTTAGGGCT-3′) and SalI-AR-Rv (5′-AAAAAAGTCGACCTGGGTGTGG-AAATAGATGG-3′), cleaved by BglII and SalI, and introduced into the BglII-SalI sites of the pEGFP-C1 vector (EGFP-AR23Q). The CAG repeat tract of EGFP-AR23Q was expanded via a method previously described (38). A primer set, BglII-AR-Fw and MmeI-AR-exp-Rv (CATCCTCACCCTGCTGCT-GCTCCAACTGCCTGGGG) was used to amplify the 5′-coding sequence including the CAG repeat tract. Another primer set, MmeI-AR-exp-Fw (AGGCCGCGAGCGCAGCACCTTC-CGACGCCAGTTTG) and AR-630Rv (TCTCCCGCTGCTG-CTGCCTT) was used to amplify the CAG tract and its 3′-flanking region. These two fragments were digested by *Mme*I (New England Biolabs), gel-purified, and treated with T4 DNA ligase to connect them at their CAG repeat tracts. The ligated fragment was gel-purified and amplified by PCR using BglII-AR-Fw and AR-630Rv primers, and digested by BglII and AflII. The resulting fragment was ligated with EGFP-AR. By two cycles of expansion, EGFP-AR45Q and EGFP-AR99Q were obtained. The N terminus fragment of AR99Q, was amplified by PCR using primers BglII-AR-Fw and SalI-AR-396Rv (AAAAAAGT-CGACGACGCAACCTCTCTCGGGGT), cleaved by BglII and SalI, and subcloned into the BglII-SalI sites of the pEGFP-C1. EGFP-DRPLA construct encoding atrophin-1 with Gln-71 was described previously (39) and was kindly provided by Dr. Masao Yamada. To prepare pcDNA3.1-tNhtt-60Q-EGFP for transient transfection, tNhtt-polyQ-EGFP fragment was cut from pIND-tNhtt-polyQ-EGFP (40) with HindIII-XbaI digestion, and the resulting fragment was inserted into pcDNA3.1-v5/His plasmid. The monomeric red fluorescence protein (mRFP) (41) and the ubiquitinated (Ub) Discosoma Red fluorescent protein (dsRed)2/N1 plasmids (42) were previously described.

Cell Culture and Treatment—Mouse neuroblastoma (Neuro2a; N2a) cells lines stably transfected with inducible expression of tNhtt-16Q-EGFP, tNhtt-60Q-EGFP, tNhtt-150Q-EGFP, and tNhtt-150Q-NLS-EGFP, which express a cDNA encoding htt exon 1 containing 16, 60 or 150 CAG repeats and fused with EGFP and eventually nuclear localization signal (NLS) (43), were previously established using the ecdysone-inducible mammalian expression system (Invitrogen) (36, 40). Neuro2a and mouse embryonic fibroblasts (MEFs) were maintained in Dulbecco's modified Eagle's medium (Invitrogen) supplemented with 10% heat-inactivated fetal bovine serum (Sigma), 100 units/ml penicillin, and 100 μg/ml streptomycin (Invitro-

Downloaded from www.jbc.org at RIKEN LIB, on December 13, 2009

Supplemental Material can be found at:
http://www.jbc.org/content/suppl/2009/03/12/M809229200.DC1.html

gen) at 37 °C in an atmosphere containing 5% CO_2 and 95% air. Neuro2a cells were induced to express tNhtt-polyQ with 1 μM ponasterone A (ponA, Invitrogen) and differentiated to neuronal phenotype with 5 mM N^6,2′-*O*-dibutyryladenosine-3′,5′-cyclic monophosphate sodium salt (dbcAMP) (Nacalai tesque). The differentiation status of the Neuro2 cells treated with dbcAMP is shown in supplemental Fig. S1. Except for the chase experiments, the cells were incubated with drugs at the time of differentiation and induction. MEFs were induced to ATG5(−/−) phenotype with 10 ng/ml doxycycline for 5 days as previously described (44).

Cells were transfected when they reached about 70–80% confluence. Transfection by Lipofectamine 2000 (Invitrogen) was done in accordance to the manufacturer's protocol in 24-well plates. Cells were used for experiments at indicated times after transfection.

Cell Death Assay—For quantification of cell death, 5 μg/ml each of Hoechst 33342 and PI were added to differentiated and induced Neuro2a cultures incubated with ROCK inhibitors. After 10 min at 37 °C, the PI-positive cells were quantified with ArrayScan (Cellomics).

RNA Interference—Each sense and antisense template short hairpin RNA (shRNA) for ROCK1 and ROCK2 was purchased from Operon, annealed and ligated into pSilencer1.0 vector with U6 promotor according to the manufacturer's instructions (Ambion). The target sequences were as follows: ROCK1, 5′-AAGTAGTGACATTGATACTAG-3′; ROCK2, 5′-AACAATAGAGATCTACAAGAT-3′. The plasmids containing shRNA were sequence-verified. Plasmids were transfected into Neuro2a cells using Lipofectamine 2000. Ater 2 days of silencing, cells were induced.

ArrayScan Quantification—For the inclusions (visible aggregates) quantification, cells were grown in 24-well plates for indicated periods, fixed in 4% paraformaldehyde, washed, and incubated with Hoechst 33258 at 1:1000 dilution in PBS. Cells were analyzed with ArrayScan®V^{TI} High Content Screening (HCS) Reader using Target Activation BioApplication (TABA). TABA analyzes images acquired with an HCS Reader and provides measurements of the intracellular fluorescence intensity and localization on a cell-by-cell basis.

In each well, more than 10,000 cells were counted and quantified for the presence of the inclusions. Nuclei stained by Hoechst 33285 provided the autofocus target and a count gave the exact number of the quantified cells. The screening itself consisted of two scans using Hoechst and fluorescein isothiocyanate (for GFP) fluorescence. First, the number of inclusions was calculated when fluorescent spots of at least 5 pixels (magnification 20× for cytoplasmic and 40× for nuclear aggregates) and an average GFP intensity of more than 1500 were labeled as inclusions. Nuclei were then defined as the objects of interest and their number determined. The percentage of the cells with inclusions was then calculated. The reliability of the inclusion quantification by ArraScan was validated by test-counting of inclusions by eyes (supplemental Fig. S2). The number of mRFP- or Ub-dsRED-positive cells and fluorescent intensity was quantified by single scan by detecting the red fluorescence of each cell in the perinuclear region within a distance of 3 pixels from the nucleus. When the average intensity exceeded 50, the cell was considered mRFP/Ub-dsRED-positive. Scanning was performed with three or four times in each experimental condition. Data were generated from the quantification of more than 250,000 cells in each experimental set-up.

TaqMan Reverse Transcriptase-PCR (RT-PCR)—Total RNA and cDNAs were prepared from Neuro2a cells as described previously (45). The TaqMan primer and probe sets were designed and synthesized based on Primer Express Software (Applied Biosystems). The nucleotide sequences of the primers for EGFP were as follows: forward 5′-AGCAAAGACCCCAACGAGAA-3′, reverse 5′-GGCGGCGGTCACGAA-3′, TaqMan probe 5′-CGCGATCACATGGTCCTGCTGG-3′; TaqMan RT-PCR was performed as described previously (46). All values obtained were normalized against the levels of β-actin using the following primers: forward 5′-TCTTTGCAGCTCCTTCGTTG-3′, reverse 5′-ATCGTCATCCATGGCGAAC-3′, TaqMan probe 5′-CGGTCCACACCCGCCACC-3′.

Chase Experiments—To determine whether soluble tNhtt-polyQ degrades faster in the presence of ROCK inhibitors, chase experiments were performed. Neuro2a cells were first differentiated and induced to express tNhtt-polyQ for 24 h in case of 16Q and 60Q and 16 h in case of 150Q cells. Thereafter, ponA was removed, the cells were washed, and incubated in a medium containing dbcAMP (for maintaining differentiation status) with either water (control) or ROCK inhibitors at 20 μM concentration for 4 or 5 days. Medium was replaced every 2 days with the same concentration of the drugs, and cells were collected everyday. The cells were subsequently lysed, and the levels of tNhtt-polyQ analyzed using Western blotting.

Western Blot Analysis—Cells were washed twice with ice-cold PBS, scraped, and resuspended in lysis buffer (0.5% Triton X-100 in PBS, 0.5 mM phenylmethylsulfonyl fluoride, Complete protease inhibitor mixture (Roche Applied Sciences). After incubating on ice for 30 min lysates were briefly sonicated. Protein concentrations were determined according to the method of Bradford using Bio-Rad protein assay reagent (Bio-Rad). Equal amounts of protein were boiled for 5 min in 2× SDS-sample buffer and then separated by 5–12% gradient SDS-PAGE and electrophoretically transferred to a polyvinylidene difluoride (polyvinylidene difluoride) membrane. The membranes were blocked in 5% skim milk in 0.05% Tween 20/Tris-buffered saline (TBS-T) and then incubated with primary antibody (dilutions in accordance with manufacturer's recommendations) overnight at 4 °C. The membranes were washed three times in TBS-T and incubated for 1 h with horseradish peroxidase-conjugated secondary antibody (dilution 1:5000). Immunoreactive proteins were detected with enhanced chemiluminescence reagents (Amersham Biosciences).

Filter Trap Assay (FTA)—FTA was performed using a Hybri-Dot manifold (Bio-Rad) and cellulose acetate membrane filter with a pore size of 0.2 μM (Advantec). The cell lysates were prepared as for Western blotting. The same amount of protein from each experimental condition was diluted to 100 μl of PBS with 2% SDS and applied to the membrane. Soluble proteins were removed by vacuum suction while the SDS-resistant aggregates stayed trapped. Wells were washed three times with 2% SDS/PBS, and suction was maintained for 20 min to allow

Downloaded from www.jbc.org at RIKEN LIB, on December 13, 2009

Supplemental Material can be found at:
http://www.jbc.org/content/suppl/2009/03/12/M809229200.DC1.html

thorough and complete trapping of SDS insoluble material. Membranes were subsequently blocked with 5% skim milk, and immunostaining was performed.

In Vitro UPS Activity Assay—Neuro2a cells were transfected with ROCK1 and/or ROCK2 shRNA and 2 days later, 10 μM MG-132 was added. Eighteen hours later, cells were collected, and 5 μg of total protein from each lysate was pipetted to 96-well plate and 100 μl of fluorogenic UPS substrate I (trypsin-like activity) or II (peptidyl glutamyl peptide hydrolase (*PGPH*)-like activity) (Calbiochem). Plates were placed in the Arvo MX 1420 Multilabel Counter (Perkin Elmer), and absorbance was detected at 460 nm.

Statistical Analysis—We used the unpaired Student's *t* test for comparison between two samples. One-way ANOVA Fisher's test followed by Tukey's HSD test or two-way ANOVA test with pairwise contrast were performed using XLSTAT or Partek Genomic Solution Software. The statistical significance was confirmed by the non-parametric Mann-Whitney test where indicated. We considered the difference between comparisons to be significant when $p < 0.05$ for all the statistical analyses.

RESULTS

ROCK Inhibitors Inhibit PolyQ Aggregation—First, we investigated whether the effect of Y-27632 on polyQ aggregation is limited to htt and AR or if it is also able to inhibit the aggregation of other polyQ-containing proteins. We found that beside htt and AR, Y-27632 decreased the aggregation of truncated and full-length ataxin-3 and atrophin-1 in a dose-dependent manner (Fig. 1). To test whether the polyQ aggregation is decreased by more ROCK inhibitors or whether it is a specific effect of Y-27632, we examined four different drugs inhibiting ROCK. The ArrayScan analysis revealed that all of them were able to decrease the polyQ aggregation in 150Q and 150Q-NLS

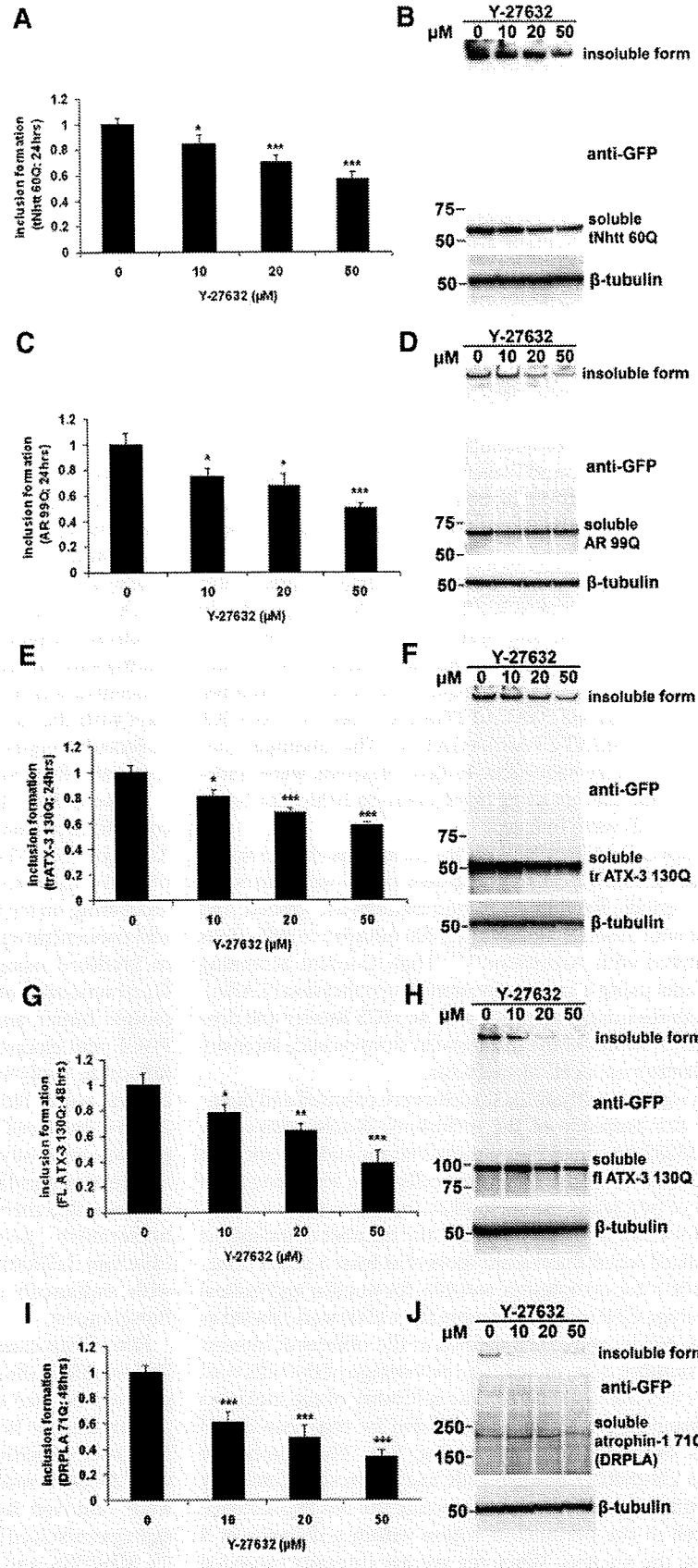

Downloaded from www.jbc.org at RIKEN LIB, on December 13, 2009

Supplemental Material can be found at:
http://www.jbc.org/content/suppl/2009/03/12/M809229200.DC1.html

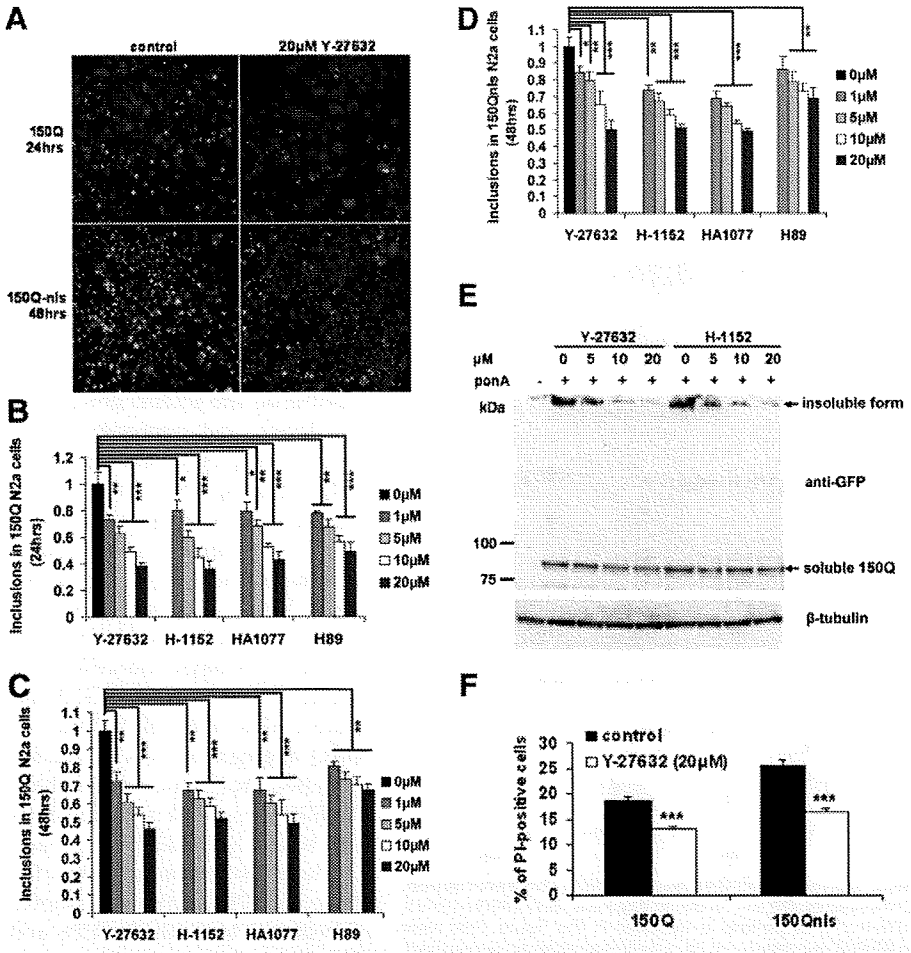

FIGURE 2. **ROCK inhibitors decrease the cytoplasmic and nuclear polyQ aggregation and toxicity in 150Q and 150Q-NLS Neuro2a cells.** Cells were plated into 24- (for ArrayScan analysis) or 12-well plates (for Western blot analysis). On the following day, cells were differentiated with 5 mM dbcAMP and induced with 1 μM ponA for different time periods as indicated in the figure and below. Cells were fixed with 4% PFA and nuclei stained with Hoechst 33258. *A*, composite image generated by ArrayScan (20× magnification) shows a clear decrease in polyQ aggregation in 150Q Neuro2a cells after 24 and 48 h by 20 μM Y-27632. *B–D*, ROCK inhibitors Y-27632, H-1152, HA1077, and H89 significantly decreased the inclusion formation rate in 150Q N2a cells 24 h (*B*) or 48 h (*C*) after induction and treatment and in 150Q-NLS N2a cells 48 h (*D*) after induction and treatment in dose-dependent manner. *E*, 150Q Neuro2a cells were plated into 12-well tissue culture plates, and the next day the cells were differentiated with 5 mM dbcAMP, induced with 1 μM ponA, and treated with Y-27632 or H-1152. Cells were collected 24-h later and processed for immunoblot analysis using anti-GFP and anti-β-tubulin antibodies. Western blot analysis showed a reduction of the soluble and insoluble 150Q in Neuro2a cells by Y-27632 and H-1152 treatment in a dose-dependent manner. *F*, cell death in 150Q and 150Q-NLS Neuro2a cells. Cells were plated into 24-well tissue culture plates, and the following day, the cells were differentiated, induced, and treated with 20 μM Y-27632. After 3 days, PI and Hoechst 33258 were added to the medium in final concentrations of 5 μg/ml. Cells were incubated for 10 min at 37 °C before ArrayScan analysis was performed. Y-27632 reduced the PI-positive cells by 31% in 150Q and 36% in 150Q-NLS Neuro2a cells ($n = 3$) as compared with untreated cells. *Bars* in *B–D* represent the relative mean values ± S.D. from four different experiments. The control value of 1 represents the control conditions with no ROCK inhibitor added to the cells. *, $p < 0.05$; **, $p < 0.005$; ***, $p < 0.001$; $p < 0.05$ by non-parametric Mann-Whitney test for significant data by ANOVA.

Neuro2a cells after 1 or 2 days of differentiation and induction in a dose-dependent manner (Fig. 2, *A–D*). The 150Q-NLS cell line was examined after 2 days because the nuclear inclusion formation sufficient for ArrayScan analysis did not appear earlier. Y-27632, H-1152, and HA1077 were very efficient in both cell lines, while H89 did not have so strong effect after 2 days of treatment. These results were confirmed by Western blot, as shown in a representative Western blot in Fig. 2*E* for Y-27632 and H-1152. Next, we examined the effect of Y-27632 on the polyQ-mediated cytotoxicity. After 3 days of 150Q and 150Q-NLS expression in Neuro2a cells, Y-27632 was able to decrease the percentage of propidium iodide-positive cells in both cell lines (Fig. 2*F*). These data confirmed the inhibitory effect of ROCK inhibitors on polyQ aggregation and polyQ cytotoxicity.

Y-27632 Decreases the Level of PolyQ Protein—Because the decrease in insoluble form of polyQ on gel top was not accompanied by an increase in the monomeric polyQ protein (Fig. 2*E*), we investigated the rate of htt expression. In 16Q Neuro2a cells, treatment with Y-27632 did not have significant effect on the protein level after 8, 12, and 24 h of induction (Fig. 3, *A* and *B* (*left panel*)). On the other hand, the level of 150Q protein decreased drastically when cells were incubated with the drug (Fig. 3, *A* and *B* (*right panel*)). The TaqMan real-time PCR showed no difference at the transcriptional level between treated and untreated cells (Fig. 3*C*).

Y-27632 Enhances the Expanded PolyQ Degradation by UPS and Autophagy—We performed a set of chase experiments to investigate

FIGURE 1. **Y-27632 reduced aggregation of different proteins with expanded polyQ.** Neuro2a cells were plated into 24- (for ArrayScan analysis) or 12-well plates (for Western blot analysis), transfected and 4-h later differentiated and treated with Y-27632. *A*, *C*, *E*, *G*, and *I*, ArrayScan analyses of the inclusion formation in Neuro2a cells transfected by plasmids coding different polyQ-containing proteins and treated with increasing concentrations of Y-27632 (10, 20, and 50 μM). Y-27632 reduced the inclusion formation of all tested proteins in a dose-dependent manner. *Bars* represent the relative mean values ± S.D. from three independent experiments. 0 μM values represent the control conditions (0 μM = 1). *, $p < 0.05$; **, $p < 0.005$; ***, $p < 0.001$. *B*, *D*, *F*, *H*, and *J*, Western blot analyses showed that Y-27632 reduced the levels of soluble and insoluble (*gel top*) forms of all tested proteins with expanded polyQ in a dose-dependent manner. *A*, and *B*, tNhtt-60Q, 24 h after transfection. *C*, and *D*, AR with 99Q, 24 h after transfection. *E*, and *F*, truncated ataxin-3 (trATX-3) with 130Q, 24 h after transfection. *G* and *H*, full-length ataxin-3 (FL ATX-3) with 130Q, 48 h after transfection. *I*, and *J*, DRPLA protein (atrophin-1) with 71Q, 48 h after transfection.

Downloaded from www.jbc.org at RIKEN LIB, on December 13, 2009

Supplemental Material can be found at:
http://www.jbc.org/content/suppl/2009/03/12/M809229200.DC1.html

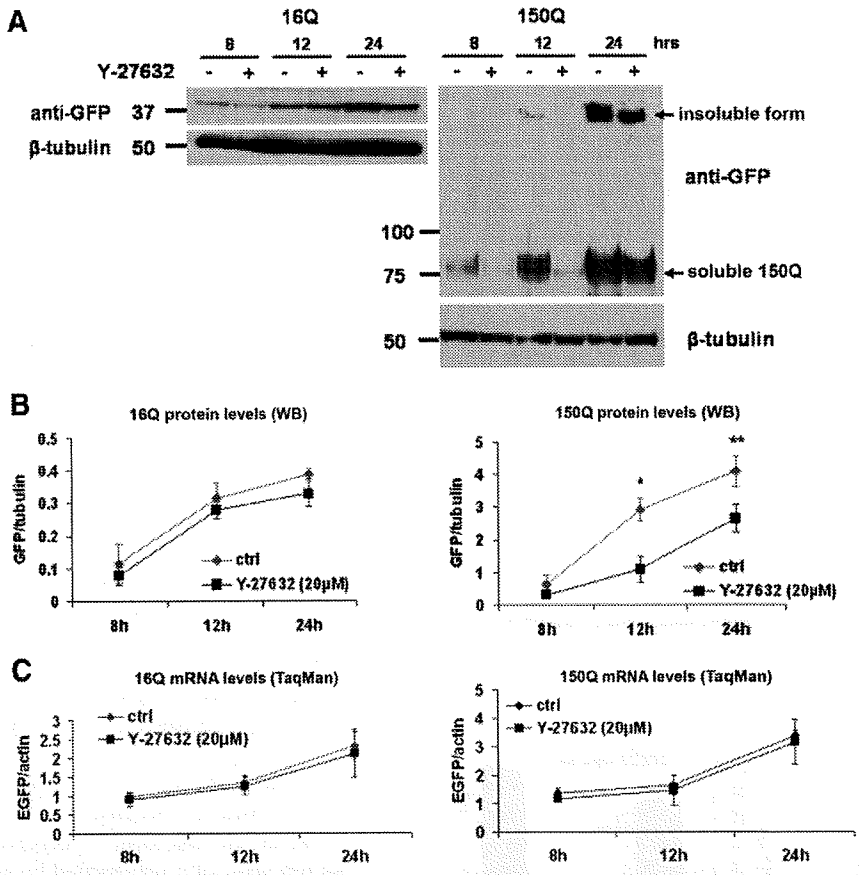

FIGURE 3. **Y-27632 decreases the levels of htt with expanded polyQ without affecting the transcription.** 16Q and 150Q Neuro2a cell were plated into 12-well plates. On the following day, cells were differentiated, induced, and treated with 20 μM Y-27632 for different time periods as indicated in the figure. Cells were collected, and total RNA for quantitative TaqMan RT-PCR or proteins for immunoblot analysis were prepared. *A*, representative Western blot showing the htt protein levels in 16Q and 150Q Neuro2a cells at different time points after induction and treatment using anti-GFP and anti-β-tubulin antibodies. *B*, quantification of band intensities of the anti-GFP immunoblots representing soluble forms of the proteins for 16Q (*left panel*) and 150Q Neuro2a cells (*right panel*) collected from three independent experiments. Levels of 16Q protein showed no significant difference between untreated and Y-27632-treated cells. Levels of soluble 150Q were significantly reduced upon Y-27632 treatment starting 12 h after induction. Data were normalized using β-tubulin. *C*, quantitative TaqMan RT-PCR analysis of the 16Q- (*left panel*) and 150Q-EGFP (*right panel*) mRNA levels showed no significant transcription alterations by 20 μM Y-27632 treatment at any time point in three independent experiments. Data were normalized using actin mRNA levels. Values in *B* and *C* are mean ± S.D. *, $p < 0.05$; **, $p < 0.005$.

the mechanistic platform of the decreased expression of expanded htt. First, we induced the expression of htt in the16Q and 60Q Neuro2a cells for 24 h, and after ponA removal, we collected the cells every 24 h. Y-27632 increased the turnover of expanded polyQ protein about 2.5 times compared with the control cells and markedly reduced the aggregation (Fig. 4, *A* and *B*). In case of 150Q, the effect on soluble form of the protein was not obvious, but the SDS-insoluble material was significantly decreased upon Y-27632 treatment (Fig. 4, *D–F*). This effect of Y-27632 was specific for expanded polyQ, because the levels of normal protein in 16Q Neuro2a cells were not affected (Fig. 4, *G* and *H*). Moreover, the drug was able to efficiently inhibit the accumulation of polyubiquitinated proteins after day 2 of the experiment (Fig. 4*A* (*bottom panel*) and *C*) suggesting the preservation of the UPS function. This data indicated that Y-27632 enhanced the degradation of mutant htt with expanded polyQ.

Next we examined which of the main degradation pathways is involved. We blocked autophagy and the UPS with 10 mM 3-methyladenine (3MA) and 10 μM MG-132, respectively (Fig. 5). The inhibition of the UPS, but not of autophagy, alleviated the effect of the drug on the soluble polyQ levels. Aggregation inhibition was partly abated when the cells were treated with 3MA or MG-132. When we blocked both pathways, the effect of Y-27632 on the soluble polyQ protein levels and aggregation was almost completely eliminated as observed using FTA (Fig. 5, *A–C*) and ArrayScan analysis (Fig. 5, *D* and *E*). To confirm this observation, we induced the ATG5(−/−) genotype in MEF 5–7 cells with doxycycline to block autophagy (Fig. 5*F*). After 5 days, the cells were transfected with 150Q-EGFP and treated. The effect of Y-27632 on polyQ aggregation was eliminated only upon the absence of autophagy (ATG5(−/−) cells) and treatment with 10 μM MG-132 (Fig. 5, *F* and *G*). These results confirmed that the effect of Y-27632 on polyQ turnover is mediated by both the UPS and autophagy.

Y-27632 Increases the Activity of UPS and Autophagy—To investigate how the degradation systems are modulated by Y-27632, we first examined UPS activity using transient transfection of ubiquitin-dsRED (Ub-dsRED) and mRFP as a control. Y-27632 reduced the accumulation of Ub-dsRED in Neuro2a cells while it did not have an effect on mRFP levels (Fig. 6, *A* and *B*). When the UPS was blocked with MG-132, the levels of Ub-dsRED more than doubled over that of the control cells, and the effect of Y-27632 fell (Fig. 6, *A* and *B*). Quantification of the Ub-dsRED- or mRFP-positive 16Q, 60Q, and 150Q Neuro2a cells by ArrayScan revealed that Y-27832 treatment significantly reduced the number of Ub-dsRED-positive cells as well as average fluorescent intensity, while it had no effect on cells transfected with mRFP (Fig. 6, *C* and *D*). These results showed that Y-27632 was able to activate the UPS in Neuro2a cells lacking mutant protein and that it alleviated the UPS block caused by expanded polyQ in 60Q and 150Q Neuro2a cells.

During autophagy, the cytosolic form of microtubule-associated protein 1 light chain 3 (LC3-I) is conjugated to phosphatidylethanolamine (PEA) to form LC3-PEA conjugate (LC3-II), which is recruited to autophagosomal mem-

Downloaded from www.jbc.org at RIKEN LIB, on December 13, 2009

Supplemental Material can be found at:
http://www.jbc.org/content/suppl/2009/03/12/M809229200.DC1.html

branes. Thus, lysosomal turnover of the autophagosomal marker LC3-II reflects autophagic activity (47). Y-27632 treatment of Neuro2a cells resulted in increased LC3-II/LC3-I ratio as observed by Western blot analysis (Fig. 6, *E* and *F*). The presented data suggested that Y-27632 is able to activate UPS and autophagy in Neuro2a cells.

ROCK1 and/or ROCK2 Knockdown Caused Activation of Degradation Systems—Knockdown of ROCKs in 150Q Neuro2a cells by shRNA resulted in reduction of polyQ aggregation (Fig. 7, *A* and *B*). ROCK1 silencing had stronger effect as compared with ROCK2 on visible aggregate formation (Fig. 7*B*). Although the knockdown of ROCK2 significantly decreased the amount of visible aggregates, we did not observe a marked decrease in insoluble fraction of 150Q on the gel top, probably because many of the large aggregates were removed by centrifugation during cell lysate preparation (Fig. 7*A*). Treatment with 20 μM Y-27632 produced additional effect at all knockdown conditions, suggesting that ROCKs are not the only targets of Y-27632 with antiaggregational activity.

Next, we investigated whether ROCKs influence the activity of the UPS and autophagy. The autophagy activity increased only when both isoforms of ROCK were silenced. Knockdown of a single ROCK had no effect on LC3-I to LC3-II conversion (Fig. 7, *A* and *C*). *In vitro* UPS activity analysis revealed that the knockdown of ROCKs activated the UPS (Fig. 7, *D* and *E*). The knockdown of ROCK1 significantly increased the trypsin-like activity, and that of ROCK2 increased the PGPH-like activity of the UPS. These results confirmed the involvement of ROCKs in the regulation of the cellular degradation pathways.

DISCUSSION

While the effect of Y-27632 on polyQ aggregation was previously identified in a screening study (32), the involvement of ROCKs was not confirmed until more recently (33, 34). In one of these reports, ROCK1 and PRK-2 were reported to be the effectors of Y-27632 in polyQ aggregation inhibition (33). The second study showed that the inhibition of profilin phosphorylation at Ser-137 by ROCK1 enhanced the direct binding of profilin to the polyproline region of htt. This interaction may sequester htt or stabilize it in a less aggregation-prone conformation. ROCK inhibitors were able to reduce the aggregation of AR as well, although the G-actin binding ability of profilin rather than direct interaction with AR appeared to be important (34).

In this report, we report on a novel effect of the ROCK inhibitor Y-27632 enhancing the clearance of mutant htt. We investigated the impact of Y-27632 on htt, AR, ataxin-3, and atrophin-1 with expanded polyQ and found a profound reduction of polyQ aggregation following Y-27632 treatment in all tested proteins. We hypothesize that in addition to previously published facts there might be yet unknown common mechanism responsible for this effect.

Therefore we investigated how mutant htt is processed after treatment with ROCK inhibitors, and found that the enhanced clearance of the expanded polyQ protein significantly contributed to the reduced polyQ aggregation. The levels of mutant htt fell markedly especially during the early phases after the induction of 150Q Neuro2a cells (Fig. 3). This change was not a consequence of modified transcription, since the TaqMan analysis showed no difference between the control and Y-27632-treated cells.

To investigate whether the decreased levels were caused by a higher turnover of the polyQ protein, we performed a set of chase experiments, which confirmed the enhanced degradation of htt (Fig. 4). Blocking of either the UPS or autophagy by MG-132 and 3MA, respectively, did not reverse the effect of Y-27632 completely. UPS inhibition suppressed the effect of the drug on the soluble form of 150Q and partially on the insoluble form. Autophagy inhibition had similar effect on the insoluble form of 150Q while the soluble form remained almost unchanged. Only simultaneous blockage of both main degradation systems reversed the effect of Y-27632 on both forms of 150Q (Fig. 5). When we overexpressed Ub-dsRED in wild type, 150Q, 60Q, or 16Q Neuro2a cell lines and treated them with Y-27632, the accumulation of Ub-dsRED markedly decreased as compared with untreated cells, suggesting the increased activity of the UPS (Fig. 6). Treatment of Neuro2a cells with Y-27832 caused enhanced conversion of LC3-I to LC3-II which suggested increased autophagy activity (Fig. 6). Our data show that the promotion of mutant htt degradation contributed in great extent to aggregation inhibition by Y-27632.

Reducing the intracellular levels of the mutant protein is the goal of many therapeutic approaches for polyQ diseases. This can be achieved by enhancing its degradation. The degradation of misfolded and damaged proteins by the UPS is essential to maintaining protein quality control, and the malfunctioning of the UPS has been linked to several neurodegenerative disorders (48). Mutant htt is a substrate of the UPS, but the presence of expanded polyQ inhibits the UPS, which results in further accumulation of htt (19–21, 41). We recently reported two drugs, amiloride and benzamil, as able to activate the UPS and enhance the clearance of mutant htt to reduce polyQ aggregation and toxicity in both the cellular and mouse models of HD (49). As well, attempts to increase the autophagic clearance of mutant htt resulted in reduced htt toxicity. Reports on several small molecules with therapeutic potential for HD activating autophagy, including rapamycin and lithium have been published (35, 50, 51). To the best of our knowledge, Y-27632 is the first chemical compound that is capable of enhancing both UPS and autophagy activity, though the effect on autophagy appeared weaker.

To investigate the direct involvement of ROCKs in the Y-27632 effect, we silenced ROCK1 and/or ROCK2. Surprisingly, both isoforms were able to reduce polyQ aggregation though the effect of ROCK1 appeared stronger (Fig. 7). Y-27632 had an additional effect in all knockdown conditions which is in agreement with the recent study identifying PRK-2 as another Y-27632 target (33). On the other hand, the effect of ROCK2 shRNA contradicts the study, which showed ROCK2 ineffective in inhibiting aggregation (33). This can be a consequence of using different methods for the aggregation detection. While the authors of the previous report utilized fluorescence resonance energy transfer (FRET), we counted visible aggregates using ArrayScan, or used immunoblotting (WB, FTA) to detect insoluble material. Further work will be necessary to clarify this discrepancy.

Downloaded from www.jbc.org at RIKEN LIB, on December 13, 2009

Supplemental Material can be found at:
http://www.jbc.org/content/suppl/2009/03/12/M809229200.DC1.html

As well, identification of downstream effectors of ROCKs influencing degradation pathways will be necessary for the development of more effective therapies. ROCK regulates the activities of many target proteins by its kinase activity. Through some proteins, such as the myosin light chain (MLC), it induces actomyosin contraction which is an important step in cytoskel-

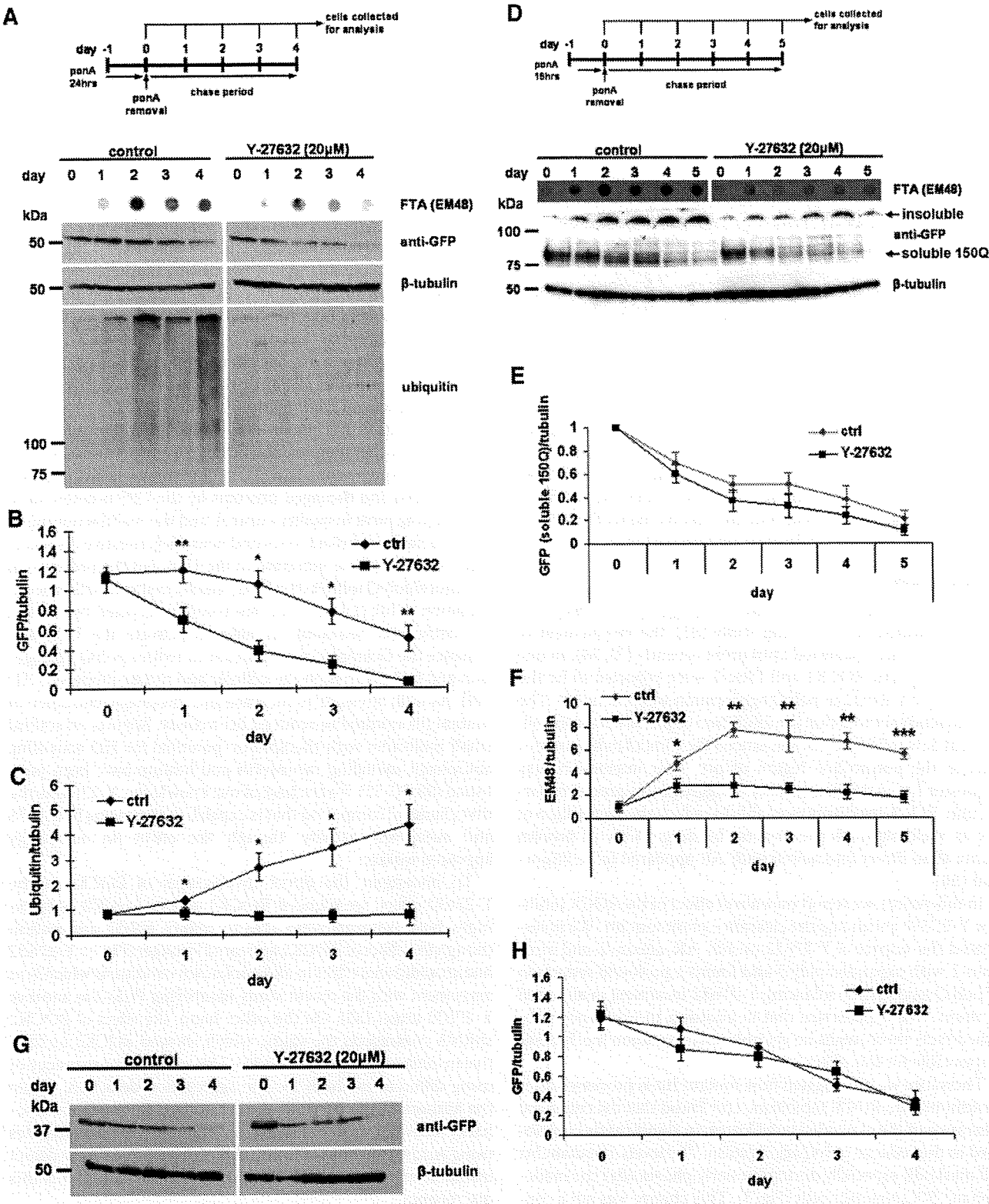

Downloaded from www.jbc.org at RIKEN LIB, on December 13, 2009

Supplemental Material can be found at:
http://www.jbc.org/content/suppl/2009/03/12/M809229200.DC1.html

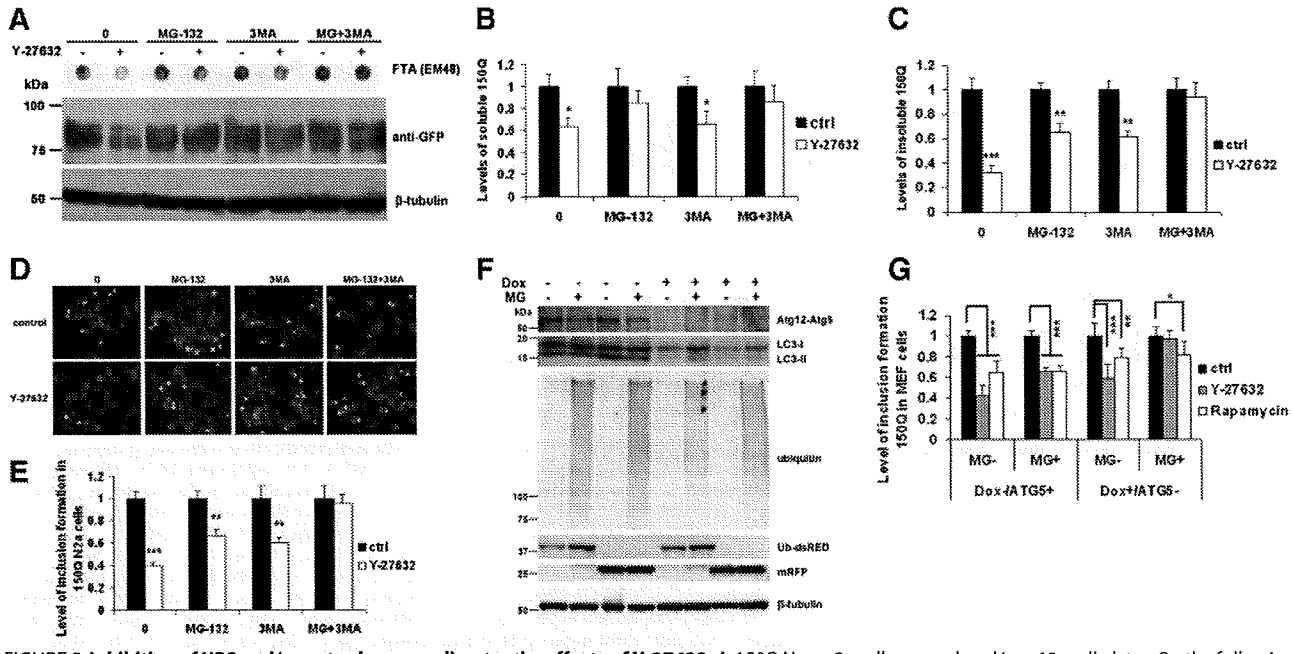

FIGURE 5. **Inhibition of UPS and/or autophagy ameliorates the effects of Y-27632.** *A*, 150Q Neuro2a cells were plated into 12-well plates. On the following day, cells were differentiated, induced, and treated with different combinations of 20 μM Y-27632, 10 μM MG-132, and 10 mM 3MA. Cells were collected 24 h later, and Western blot and FTA analysis were performed using anti-GFP, anti-β-tubulin, and EM48 antibodies. *B*, quantification of the 150Q band intensities in Western blot revealed that the inhibition of UPS but not that of autophagy ameliorated the effect of Y-27632 on soluble protein. *C*, densitometric quantification of FTA showed that the combination of the UPS and macroautophgy blockage was necessary to abolish the effect of Y-27632 on the accumulation of the insoluble form of 150Q. Inhibition of each of the degradation pathways separately ameliorated only partly the effect of Y-27632. Densitometric data were normalized using β-tubulin. *D*, 150Q Neuro2a cells were treated as described above and processed for the ArrayScan analysis. Compound images generated by ArrayScan show the effect of degradation pathways block on Y-27632-mediated polyQ aggregation. *E*, ArrayScan analysis quantification supported the data obtained by FTA analysis. *F*, MEF 5–7 cells were treated with 10 ng/ml doxycycline for 5 days to knockdown Atg5 and inhibit autophagy. To demonstrate the UPS inhibition by 10 μM MG-132 (*MG*), cells were transfected with ubiquitinated dsRED (*Ub-dsRED*) or mRFP and treated with MG for 1 day. Western blot analysis using anti-Atg5 antibody showed almost complete absence of Atg5 protein (in complex with Atg12) in doxycycline-treated cells. Anti-LC3 immunoblot revealed the consequent lack of autophagy activity in these cells. The levels of polyubiquitinated proteins and Ub-dsRED increased in cells treated with MG, while mRFP levels remained unchanged. *G*, untreated and doxycycline-treated MEF 5–7 cells were plated into 6-well plates and next day transfected with tNhtt-150Q-EGFP. Cells were then treated with 20 μM Y-27632 or 0.2 μM rapamycin and/or 10 μM MG-132 for 24 h. ArrayScan analysis confirmed that only the simultaneous inhibition of both UPS and autophagy negated the effect of Y-27632 (in dox +/Atg5- cells treated with MG-132 (*MG*)). Rapamycin, an mTOR inhibitor, activates autophagy and was used as a control. *Bars* represent the relative mean values ± S.D. from three independent experiments. The control value of 1 represents the control conditions without Y-27632 (*B*, *C*, and *E*) or without Y-27632 and rapamycin treatment (*G*). *, $p < 0.05$; **, $p < 0.005$; ***, $p < 0.001$.

etal rearrangements (52). ROCK phosphorylates LIM kinases enhancing their activity, and the subsequent phosphorylation of cofilin proteins blocks their F-actin-severing activity (53–55). Another ROCK substrate, collapsin response mediator protein-2 (CRMP-2), is also involved in the regulation of cytoskeletal reorganization (56, 57). Taken together, ROCK activation leads directly to a number of actin-myosin-mediated processes including cell motility, adhesion, phagocytosis, neurite retraction, and smooth muscle contraction. These questions are thus raised: how does the cytoskeleton affect the activity of UPS and/or autophagy? Which of the ROCK targets are involved in this process?

We have observed that chemical ROCK inhibition efficiently disrupted aggresome formation in Neuro2a cells both in the presence and absence of htt with expanded polyQ (data not shown). Aggresome formation is a cellular response when UPS is overloaded by the production of aggregation-prone misfolded proteins (58) or UPS is chemically inhibited (59). ROCK has also been reported as a regulator of intracellular redistribution of lysosomes in invasive tumor cells (60), as we observed in

FIGURE 4. **Y-27632 enhances the degradation of htt with expanded polyQ.** 16Q, 60Q, and 150Q Neuro2a cells were plated into 12-well plates and 1-day later differentiated with dbcAMP and induced with ponA. After 24 h in 16Q and 60Q cells and 16 h in 150Q Neuro2a cells, expression of htt polyQ was shut down by ponA removal, and cells were treated with 20 μM Y-27632 for the time periods indicated in the figure. Cells were collected and processed for immunoblot analysis using EM48, anti-GFP, anti-β-tubulin, or anti-ubiquitin antibodies. *A*, Western blot and FTA analysis of the chase experiment in 60Q Neuro2a cells showed enhanced degradation of soluble 60Q (anti-GFP) and reduced accumulation of the insoluble form of the protein (EM48; FTA) upon treatment with Y-27632. The *top panel* displays the experimental design of the chase experiments in 60Q and 16Q Neuro2a cells. *B*, densitometric quantification of a Western blot confirmed significant augmentation of soluble 60Q degradation in cells treated with Y-27632 comparing to untreated cells. *C*, quantification of ubiquitin immunoreactivity showed no accumulation of polyubiquitinated proteins in Y-27632-treated cells in contrast to untreated cells. *D*, Western blot and FTA analysis of the chase experiment in 150Q Neuro2a cell line revealed reduced accumulation of the insoluble form of the protein (anti-GFP, gel top in Western blot; EM48, FTA) by Y-27632 treatment. The *top panel* displays the experimental design of the chase experiment in 150Q Neuro2a cells. *E*, densitometric quantification of the soluble 150Q levels (anti-GFP, Western blot) revealed no significant difference between treated and untreated cells. *F*, quantification of the SDS-insoluble (aggregated) 150Q (EM48, FTA) exhibited a marked increase of the insoluble protein clearance in Y-27632-treated cells. *G*, Western blot analysis of the chase experiment in 16Q Neuro2a cell line. *H*, densitometric quantification revealed no difference of 16Q degradation between treated and untreated cells. All data were normalized using β-tubulin. All presented values are mean ± S.D. from three independent experiments. *, $p < 0.05$; **, $p < 0.005$.

Downloaded from www.jbc.org at RIKEN LIB, on December 13, 2009

Supplemental Material can be found at:
http://www.jbc.org/content/suppl/2009/03/12/M809229200.DC1.html

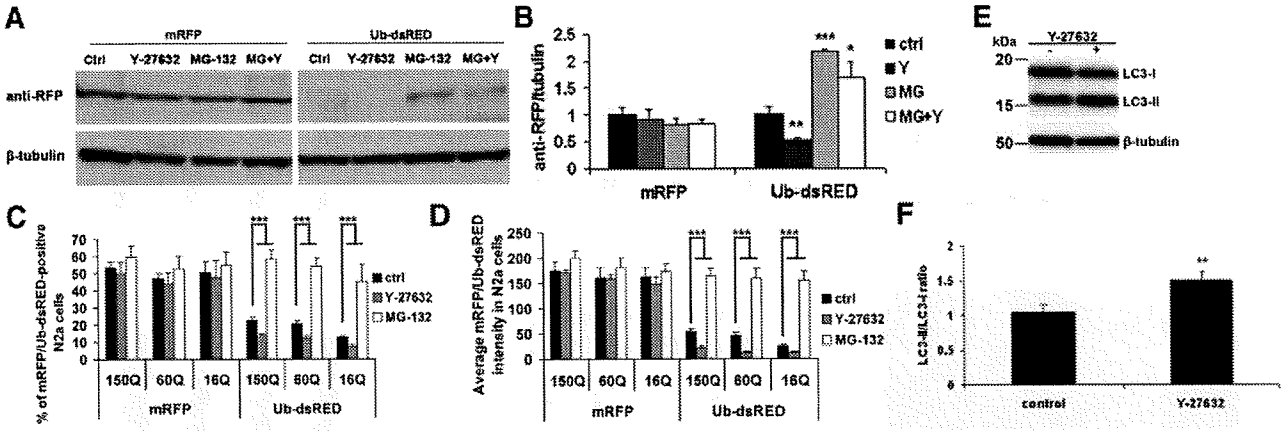

FIGURE 6. **Y-27632 increases the UPS and autophagy activity.** *A*, wild type Neuro2a cells were plated into 12-well plates. On the following day, cells were transfected with mRFP or Ub-dsRED and 4-h later differentiated and treated with 20 μM Y-27632 and/or 10 μM MG-132 for additional 24 h. Cells were then processed for immunoblot with anti-RFP and anti-β-tubulin. *B*, Western blot quantification confirmed that Y-27632 significantly decreased the levels of Ub-dsRED but not mRFP. *C* and *D*, 150Q, 60Q, and 16Q Neuro2a cells were plated into 24-well plates and transfected in a similar manner as described in *A*. Four hours later, the cells were differentiated, induced, and treated with drugs. ArrayScan analysis revealed that the percentage of Ub-dsRED-positive cells (*C*) and average red fluorescence in the cells (*D*) decreased in Y-27632-treated cells. Y-27632 had no effect on mRFP fluorescence. *E*, wild type Neuro2a cells were plated into 6-well plates, and 1-day later, cells were left untreated or treated with 20 μM Y-27632 for 24 h and processed for Western blot analysis of the LC3 conversion. *F*, densitometric quantification confirmed that Y-27632 significantly increased the conversion of LC3 representing increased autophagic activity in the treated cells. *Bars* in *B* and *F* represent the relative mean values ± S.D. from three independent experiments. The control value of 1 represents the control conditions without Y-27632 treatment. *Bars* in *C* and *D* represent mean values ± S.D. from three independent experiments. *, $p < 0.05$; **, $p < 0.005$; ***, $p < 0.001$.

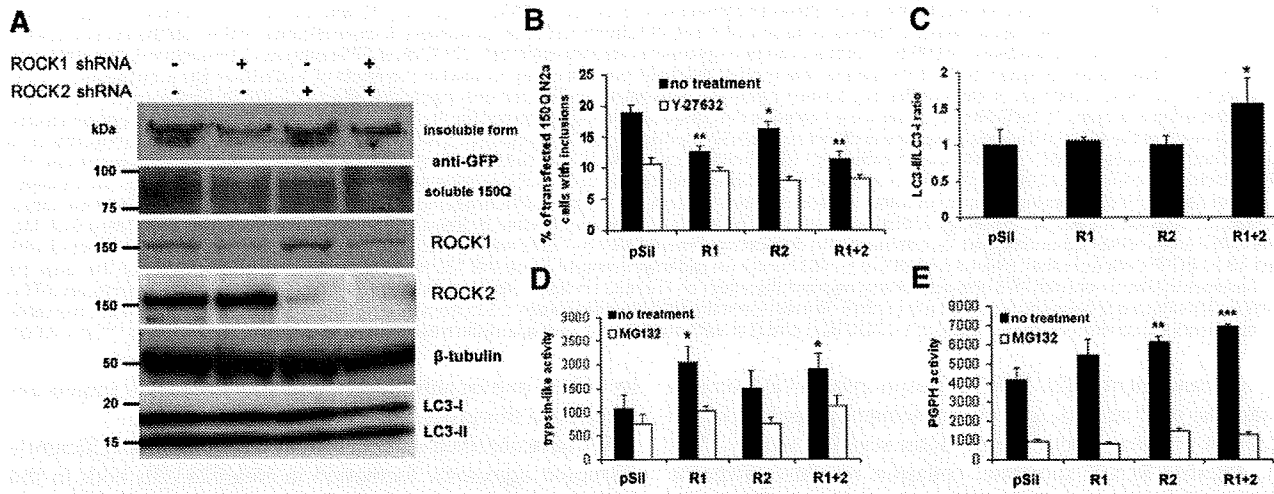

FIGURE 7. **Knockdown of ROCK1 and/or ROCK2 reduces polyQ aggregation and activates the main degradation pathways in 150Q Neuro2a cells.** 150Q Neuro2a cells were plated into 12-well plates and 1-day later transfected with different combinations of pSil vector, ROCK1 (R2) and ROCK2 (R2) shRNA (+mRFP as the transfection marker). After 4 h, the cells were differentiated for 48 h, then induced, and eventually treated with 20 μM Y-27632. Cells were processed 24 h later for Western blot or ArrayScan analysis. *A*, immunoblot using anti-GFP, anti-ROCK1, anti-ROCK2 antibodies showed decreased levels of 150Q (especially the soluble form) upon ROCKs silencing. LC3 conversion was enhanced only in the absence of both ROCKs. *B*, ArrayScan analysis showed a significant reduction of 150Q inclusion formation by ROCKs silencing. Y-27632 treatment had an additional affect in all ROCK knockdown conditions. *C*, quantification of the band intensities of LC3 blots revealed enhanced conversion of LC3 when both ROCK isoforms were knocked down. *D* and *E*, ROCKs knockdown was implemented in a similar manner as described above. After 2 days, cells were left untreated or treated with 10 μM MG-132 (for assay control) and incubated for 18 h. Cell lysates were then prepared for *in vitro* UPS activity assays. Knockdown of ROCK1 caused activation of trypsin-like activity, while ROCK2 appeared to be responsible for the PGPH activity of the UPS. The y axis represents the absorbance at 460 nm. *Bars* in *B*, *D*, and *E* represent mean values ± S.D., and *bars* in *C* represent the relative mean values ± S.D. from three independent experiments. The control value of 1 in *C* represents the control cells transfected with empty pSil vector. *, $p < 0.05$; **, $p < 0.005$; ***, $p < 0.001$.

Neuro2a cells (data not shown). The treatment of Neuro2a cells with Y-27632 hindered subcellular spreading of the lysosomes and promoted recruitment of the lysosomes in the perinuclear region. It is not clear however, if this redistribution contributes to the activation of autophagy, a matter still under investigation.

Another possible link between ROCKs and autophagy is the involvement of ROCKs in Akt signaling (27). Akt activation was shown to inhibit the mTOR-dependent autophagy activity in some cell lines including Neuro2a (61–63). Moreover, one recent study identified an actin-related protein (Arp2) to be a link between the actin cytoskeleton and autophagic machinery (64).

The downstream substrates responsible for degradation machinery activation are unknown and are the subjects of further investigation. This may potentially lead to identification or

Downloaded from www.jbc.org at RIKEN LIB, on December 13, 2009

Supplemental Material can be found at:
http://www.jbc.org/content/suppl/2009/03/12/M809229200.DC1.html

development of more potent and specific inhibitors providing effective treatment for polyQ-related diseases.

Acknowledgments—We thank Dr. Noboru Mizushima for the MEF 5–7 cell line and anti-ATG5 antibody. Also, we thank Dr. Masao Yamada for DRPLA (atrophin-1) plasmids. We would like to thank David W. Chapmon for the stylistic corrections in the manuscript.

REFERENCES

1. Myers, R. H. (2004) *NeuroRX*, **1,** 255–262
2. The Huntington's Disease Collaborative Research Group (1993) *Cell* **72,** 971–983
3. Orr, H. T., and Zoghbi, H. Y. (2007) *Annu. Rev. Neurosci.* **30,** 575–621
4. Leavitt, B. R., van Raamsdonk, J. M., Shehadeh, J., Fernandes, H., Murphy, Z., Graham, R. K., Wellington, C. L., Raymond, L. A., and Hayden, M. R. (2006) *J. Neurochem.* **96,** 1121–1129
5. Davies, S. W., Turmaine, M., Cozens, B. A., DiFiglia, M., Sharp, A. H., Ross, C. A., Scherzinger, E., Wanker, E. E., Mangiarini, L., and Bates, G. P. (1997) *Cell* **90,** 537–548
6. DiFiglia, M., Sapp, E., Chase, K. O., Davies, S. W., Bates, G. P., Vonsattel, J. P., and Aronin, N. (1997) *Science* **277,** 1990–1993
7. Landles, C., and Bates, G. P. (2004) *EMBO Rep.* **5,** 958–963
8. Yamanaka, T., Miyazaki, H., Oyama, F., Kurosawa, M., Washizu, C., Doi, H., and Nukina, N. (2008) *EMBO J.* **27,** 827–839
9. Kegel, K. B., Meloni, A. R., Yi, Y., Kim, Y. J., Doyle, E., Cuiffo, B. G., Sapp, E., Wang, Y., Qin, Z. H., Chen, J. D., Nevins, J. R., Aronin, N., and DiFiglia, M. (2002) *J. Biol. Chem.* **277,** 7466–7476
10. Nucifora, F. C., Jr., Sasaki, M., Peters, M. F., Huang, H., Cooper, J. K., Yamada, M., Takahashi, H., Tsuji, S., Troncoso, J., Dawson, V. L., Dawson, T. M., and Ross, C. A. (2001) *Science* **291,** 2423–2428
11. Steffan, J. S., Kazantsev, A., Spasic-Boskovic, O., Greenwald, M., Zhu, Y. Z., Gohler, H., Wanker, E. E., Bates, G. P., Housman, D. E., and Thompson, L. M. (2000) *Proc. Natl. Acad. Sci. U. S. A.* **97,** 6763–6768
12. Lee, W. C., Yoshihara, M., and Littleton, J. T. (2004) *Proc. Natl. Acad. Sci. U. S. A.* **101,** 224–3229
13. Li, H., Li, S. H., Johnston, H., Shelbourne, P. F., and Li, X. J. (2000) *Nat. Genet.* **25,** 385–389
14. Usdin, M. T., Shelbourne, P. F., Myers, R. M., and Madison, D. V. (1999) *Hum. Mol. Genet.* **8,** 839–846
15. Beal, M. F. (2005) *Ann. Neurol.* **58,** 495–505
16. Ross, C. A. (2002) *Neuron* **35,** 819–822
17. Evert, B. O., Wullner, U., and Klockgether, T. (2000) *Cell Tissue Res.* **301,** 189–204
18. Davies, J. E., Sarkar, S., and Rubinsztein, D. C. (2007) *BMC Biochem.* **8,** S2
19. Bence, N. F., Sampat, R. M., and Kopito, R. R. (2001) *Science* **292,** 1552–1555
20. Jana, N. R., Zemskov, E. A., Wang, G., and Nukina, N. (2001) *Hum. Mol. Genet.* **10,** 1049–1059
21. Bennett, E. J., Bence, N. F., Jayakumar, R., and Kopito, R. R. (2005) *Mol. Cell* **17,** 351–365
22. Ishizaki, T., Maekawa, M., Fujisawa, K., Okawa, K., Iwamatsu, A., Fujita, A., Watanabe, N., Saito, Y., Kakizuka, A., Morii, N., and Narumiya, S. (1996) *EMBO J.* **15,** 1885–1893
23. Leung, T., Manser, E., Tan, L., and Lim, L. (1995) *J. Biol. Chem.* **270,** 29051–29054
24. Matsui, T., Amano, M., Yamamoto, T., Chihara, K., Nakafuku, M., Ito, M., Nakano, T., Okawa, K., Iwamatsu, A., and Kaibuchi, K. (1996) *EMBO J.* **15,** 2208–2216
25. Riento, K., and Ridley, A. J. (2003) *Nat. Rev. Mol. Cell Biol.* **4,** 446–456
26. Denker, S. P., Huang, D. C., Orlowski, J., Furthmayr, H., and Barber, D. L. (2000) *Mol. Cell* **6,** 1425–1436
27. Li, Z., Dong, X., Wang, Z., Liu, W., Deng, N., Ding, Y., Tang, L., Hla, T., Zeng, R., Li, L., and Wu, D. (2005) *Nat. Cell Biol.* **7,** 399–404
28. Zhou, Y., Su, Y., Li, B., Liu, F., Ryder, J. W., Wu, X., Gonzalez-DeWhitt, P. A., Gelfanova, V., Hale, J. E., May, P. C., Paul, S. M., and Ni, B. (2003) *Science* **302,** 1215–1217
29. Pedrini, S., Carter, T. L., Prendergast, G., Petanceska, S., Ehrlich, M. E., and Gandy, S. (2005) *PLoS Med.* **2,** e18
30. Qin, W., Yang, T., Ho, L. Zhao, Z., Wang, J., Chen, L., Zhao, W., Thiyagarajan, M., MacGrogan, D., Rodgers, J. T., Puigserver, P., Sadoshima, J., Deng, H., Pedrini, S., Gandy, S., Sauve, A. A., and Pasinetti, G. M. (2006) *J. Biol. Chem.* **281,** 21745–21754
31. Satoh, S., Toshima, Y., Hitomi, A., Ikegaki, I., Seto, M., and Asano, T. (2008) *Brain Res.* **1193,** 102–108
32. Pollitt, S. K., Pallos, J., Shao, J., Desai, U. A., Ma, A. A. K., Thompson, L. M., Marsh, J. L., and Diamond, M. I. (2003) *Neuron* **40,** 685–694
33. Shao, J., Welch, W. J., and Diamond, M. I. (2008) *FEBS Lett.* **582,** 1637–1642
34. Shao, J., Welch, W. J., Dispropero, N. A., and Diamond, M. I. (2008) *Mol. Cell Biol.* **28,** 5196–5208
35. Ravikumar, B., Vacher, C., Berger, Z., Davies, J. E., Luo, S., Oroz, L. G., Scaravilli, F., Easton, D. F., Duden, R., O'Kane, C. J., and Rubinsztein, D. C. (2004) *Nat. Genet.* **36,** 585–595
36. Wang, G. H., Mitsui, K., Kotliarova, S., Yamashita, A., Nagao, Y., Tokuhiro, S., Iwatsubo, T., Kanazawa, I., and Nukina, N. (1999) *Neuroreport* **10,** 2435–2438
37. Wang, G. H., Sawai, N., Kotliarova, S., Kanazawa, I., and Nukina, N. (2000) *Hum. Mol. Genet.* **9,** 1795–1803
38. Peters, M. F., and Ross, C. A. (1999) *Neurosci. Lett.* **275,** 129–132
39. Tadokoro, K., Yamazaki-Inoue, M., Tachibana, M., Fujishiro, M., Nagao, K., Toyoda, M., Ozaki, M., Ono, M., Miki, N., Miyashita, T., and Yamada, M. (2005) *J. Hum. Genet.* **50,** 382–394
40. Zemskov, E. A., Jana, N. R., Kurosawa, M., Miyazaki, H., Sakamoto, N., Nekooki, M., and Nukina, N. (2003) *J. Neurochem.* **87,** 395–406
41. Machida, Y., Okada, T., Kurosawa, M., Oyama, F., Ozawa, K., and Nukina, N. (2006) *Biochem. Biophys. Res. Commun.* **343,** 190–197
42. Khan, L. A., Bauer, P. O., Miyazaki, H., Lindenberg, K. S., Landwehrmeyer, B. G., and Nukina, N. (2006) *J. Neurochem.* **98,** 576–587
43. Doi, H., Mitsui, K., Kurosawa, M., Machida, Y., Kuroiwa, Y., and Nukina, N. (2004) *FEBS Lett.* **571,** 171–176
44. Hosokawa, N., Hara, Y., and Mizushima, N. (2006) *FEBS Lett.* **580,** 2623–2629
45. Oyama, F., Kotliarova, S., Harada, A., Ito, M., Miyazaki, H., Ueyama, Y., Hirokawa, N., Nukina, N., and Ihara, Y. (2004) *J. Biol. Chem.* **279,** 27272–27277
46. Kotliarova, S., Jana, N. R., Sakamoto, N., Kurosawa, M., Miyazaki, H., Nekooki, M., Doi, H., Machida, Y., Wong, H. K., Suzuki, T., Uchikawa, C., Kotliarov, Y., Uchida, K., Nagao, Y., Nagaoka, U., Tamaoka, A., Oyanagi, K., Oyama, F., and Nukina, N. (2005) *J. Neurochem.* **93,** 641–653
47. Asanuma, K., Tanida, I., Shirato, I., Ueno, T., Takahara, H., Nishitani, T., Kominami, E., and Tomino, Y. (2003) *FASEB J.* **17,** 1165–1167
48. Ross, C. A., and Pickart, C. M. (2004) *Trends Cell Biol.* **14,** 703–711
49. Wong, H. K., Bauer, P. O., Kurosawa, M., Goswami, A., Washizu, C., Machida, Y., Tosaki, A., Yamada, M., Knopfel, T., Nakamura, T., and Nukina, N. (2008) *Hum. Mol. Genet.* **17,** 3223–3235
50. Sarkar, S., Krishna, G., Imarisio, S., Saiki, S., O'Kane, C. J., and Rubinsztein, D. C. (2004) *Hum. Mol. Genet.* **17,** 170–178
51. Zhang, L., Yu, J., Pan, H., Hu, P., Hao, Y., Cai, W., Zhu, H., Yu, A. D., Xie, X., Ma, D., and Yuan, J. (2007) *Proc. Natl. Acad. Sci. U. S. A.* **104,** 19023–19028
52. Brown, M. E., and Bridgman, P. C. (2004) *J. Neurobiol.* **58,** 118–130
53. Ohashi, K., Nagata, K., Maekawa, M., Ishizaki, T., Narumiya, S., and Mizuno, K. (2000) *J. Biol. Chem.* **275,** 3577–3582
54. Sumi, T., Matsumoto, K., and Nakamura, T. (2001) *J. Biol. Chem.* **276,** 670–676
55. Scott, R. W., and Olson, M. F. (2007) *J. Mol. Med.* **85,** 555–568
56. Arimura, N., Inagaki, N., Chihara, K., Ménager, C., Nakamura, N., Amano, M., Iwamatsu, A., Goshima, Y., and Kaibuchi, K. (2000) *J. Biol. Chem.* **275,** 23973–23980
57. Arimura, N., Menager, C., Fukata, Y., and Kaibuchi, K. (2004) *J. Neurobiol.* **58,** 34–47
58. Johnston, J. A., Ward, C. L., and Kopito, R. R. (1998) *J. Cell Biol.* **143,**

Downloaded from www.jbc.org at RIKEN LIB, on December 13, 2009

Supplemental Material can be found at:
http://www.jbc.org/content/suppl/2009/03/12/M809229200.DC1.html

1883–1898
59. Nagaoka, U., Kim, K., Jana, N. R., Doi, H., Maruyama, M., Mitsui, K., Oyama, F., and Nukina, N. (2004) *J. Neurochem.* **91,** 57–68
60. Nishimura, Y., Itoh, K., Yoshioka, K., Uehata, M., and Himeno, M. (2000) *Cell Tissue Res.* **301,** 341–351
61. Kuo, P. L., Hsu, Y. L., and Cho, C. Y. (2006) *Mol. Cancer Ther.* **5,** 3209–3221
62. Degtyarev, M., De Maziere, A., Orr, C., Lin, J., Lee, B. B., Tien, J. Y., Prior, W. W., van Dijk, S., Wu, H., Gray, D. C., Davis, D. P., Stern, H. M., Murray, L. J., Hoeflich, K. P., Klumperman, J., Friedman, L. S., and Lin, K. (2008) *J. Cell Biol.* **183,** 101–116
63. Zeng, M., and Zhou, J. N. (2008) *Cell Signal.* **20,** 659–665
64. Monastyrska, I., He, C., Geng, J., Hoppe, A. D., Li, Z., and Klionsky, D. J. (2008) *Mol. Biol. Cell* **19,** 1962–1975

ASBMB The Journal of Biological Chemistry

Downloaded from www.jbc.org at RIKEN LIB, on December 13, 2009

Neurobiology of Disease

Cross-Seeding Fibrillation of Q/N-Rich Proteins Offers New Pathomechanism of Polyglutamine Diseases

Yoshiaki Furukawa, Kumi Kaneko, Gen Matsumoto, Masaru Kurosawa, and Nobuyuki Nukina
Laboratory for Structural Neuropathology, Brain Science Institute, RIKEN, Wako, Saitama 351-0198, Japan

A pathological hallmark of the Huntington's disease (HD) is intracellular inclusions containing a huntingtin (Htt) protein with an elongated polyglutamine tract. Aggregation of mutant Htt causes abnormal protein–protein interactions, and the functional dysregulation of aggregate-interacting proteins (AIPs) has been proposed as a pathomechanism of HD. Despite this, a molecular mechanism remains unknown how Htt aggregates sequester AIPs. We note an RNA-binding protein, TIA-1, as a model of AIPs containing a Q/N-rich sequence and suggest that *in vitro* and *in vivo* Htt fibrillar aggregates function as a structural template for inducing insoluble fibrillation of TIA-1. It is also plausible that such a cross-seeding activity of Htt aggregates represses the physiological function of TIA-1. We thus propose that Htt aggregates act as an intracellular hub for the cross-seeded fibrillation of Q/N-rich AIPs and that a cross-seeding reaction is a molecular origin to cause diverse pathologies in a polyglutamine disease.

Introduction

Huntington's disease (HD) is a neurodegenerative disorder caused by an abnormal expansion of CAG repeats located in exon I of the HD gene (Zoghbi and Orr, 2000). The CAG repeat encodes a polyglutamine [poly(Q)] stretch in the HD gene product, huntingtin (Htt), and is highly polymorphic; 6–34 repeats in unaffected individuals, but >36 repeats in HD patients (Zoghbi and Orr, 2000). Compared with other neurodegenerative diseases such as Alzheimer's disease, a disease pathology seem more diverse in HD: namely, a wider variety of cellular systems including protein degradation, transcription, and RNA metabolism become dysfunctional (Zoghbi and Orr, 2000).

Several pathomechanisms of HD have been proposed based on a high propensity of an expanded poly(Q) for aggregation, which is evidenced by the observation that mutant Htt is deposited as inclusion bodies inside affected neurons (Davies et al., 1997). Although it remains unclear whether Htt aggregates themselves exert neurotoxicity, mutant Htt has been proposed to sequester many other proteins [aggregate-interacting proteins (AIPs)] including glutamine (Q)/asparagine (N)-rich proteins, leading to cellular dysfunction (Nucifora et al., 2001; Schaffar et al., 2004). Given some of these AIPs remain entrapped in Htt aggregates even after harsh treatment with a strong ionic detergent (Mitsui et al., 2002), irreversible interactions with mutant Htt will be detrimental to physiological functions of AIPs. It is thus tempting to speculate that dysfunction of various AIPs on coaggregation with Htt produces pathological diversity of HD. Despite this, a molecular mechanism underlying coaggregation of AIPs with mutant Htt remains an open question.

Htt with an expanded poly(Q) tract forms insoluble, amyloid-like fibrillar aggregates (Scherzinger et al., 1997). A preformed fibril can act as a seed that significantly accelerates the transition from a soluble protein into an insoluble fibril, and a seed accelerates fibrillation of the same protein molecule with a seed constituent (Harper and Lansbury, 1997). Seeding reactions also occur between different kinds of protein molecules with low sequence identity, albeit with low efficiency in general, which is called as a cross-seeding reaction (O'Nuallain et al., 2004). Unlike a transient association with aggregates, we hypothesize that a possible cross-seeding reaction of Htt integrates some of AIPs into very rigid structure of Htt fibrils, thereby resulting in the functional inactivation of integrated AIPs. To understand the coaggregation process at a molecular level, we note T-cell intracellular antigen-1 (TIA-1) as a model of AIPs in poly(Q) diseases (Waelter et al., 2001).

In this study, we have revealed that TIA-1 is sequestered in inclusions in a HD model mouse. Although TIA-1 contains no poly(Q) tract (at most three consecutive glutamines) in its primary sequence, our results show that *in vitro* Htt aggregates efficiently seed the fibrillation of TIA-1 through a C-terminal Q/N-rich domain of TIA-1. Using a cultured cell model, we also show that the coaggregation of TIA-1 with mutant Htt decreases amounts of soluble TIA-1 and represses the TIA-1 function as a translational silencer. We thus propose that Htt aggregates act as a hub for recruiting cellular components through a cross-seeding mechanism.

Materials and Methods

Preparation of recombinant proteins. For facilitation of protein purification, a 6× His tag was introduced at the N terminus of glutathione-*S*-transferase (GST) (a pGEX6P-2 vector; GE Healthcare). GST-Htt42Q was expressed in *Escherichia coli* (Rosetta) by 0.1 mM isopropyl β-D-

Received Feb. 16, 2009; accepted March 23, 2009.

This work was supported by Ministry of Education, Culture, Sports, Science, and Technology of Japan Grant-in-Aid 17025044 for Scientific Research on Priority Areas (Research on Pathomechanisms of Brain Disorders) (N.N.) and Grant-in-Aid 18031044 (Y.F.), and Ministry of Health, Welfare, and Labor (Japan) Grant-in-Aid for the Research on Measures for Intractable Diseases (N.N.). We thank Dr. Shoji Watanabe for technical assistance and fruitful discussion.

Correspondence should be addressed to Nobuyuki Nukina, Laboratory for Structural Neuropathology, Brain Science Institute, RIKEN, 2-1 Hirosawa, Wako, Saitama 351-0198, Japan. E-mail: nukina@brain.riken.jp.

DOI:10.1523/JNEUROSCI.0783-09.2009

Copyright © 2009 Society for Neuroscience 0270-6474/09/295153-10$15.00/0

thiogalactoside (IPTG) at 20°C for 2 d and purified with Proteus Midi IMAC (Pro-Chem) and glutathione Sepharose (GE Healthcare). TIA-1^{C} (Met 310 to Gln 406) was also N-terminally fused with a His-tagged GST protein, and its expression in *E. coli* (Rosetta) was induced by 1 mM IPTG at 37°C for 6 h. GST-TIA-1^{C} was obtained as inclusion bodies and purified with Proteus Midi IMAC in the presence of 8 M urea. Refolding of GST-TIA-1^{C} was performed by 60-fold dilution in 20 mM Tris/100 mM NaCl/5 mM DTT/1 mM EDTA, pH 9, with stirring overnight at 4°C. TIA-1^{FL} and TIA-1^{N} (Met 1 to Asp 309) were cloned using a vector, pET15b (Novagen), and the expression in *E. coli* (Rosetta) was induced by 0.4 mM IPTG and 0.4% glucose at 30°C for 3 h. Both proteins remain in a soluble fraction and were purified with Proteus Midi IMAC. Protein concentration was determined spectroscopically: 42,860 cm^{-1} M^{-1} (GST-Htt42Q), 83,770 cm^{-1} M^{-1} (GST-TIA-1^{C}), 80,330 cm^{-1} M^{-1} (TIA-1^{FL}), and 39,420 cm^{-1} M^{-1} (TIA-1^{N}) of an extinction coefficient at 280 nm.

For modification with thiol-specific Alexa dyes, all four Cys residues in GST are mutated to Ser (GST^{noCys}), and a unique Cys residue was further introduced at the N terminus of Htt42Q or TIA-1^{C}. In 50 mM Tris/8 M urea/1 mM tris(2-carboxyethyl)phosphine (TCEP)/1 mM EDTA, pH 7.0, 250 μM GST^{noCys}-Cys-Htt42Q or GST^{noCys}-Cys-TIA-1^{C} was incubated with 1 mM Alexa 555 or Alexa 488 maleimide (Invitrogen) for 1 h at room temperature, respectively. Modified proteins were refolded with 60-fold dilution and overnight stirring in 20 mM Tris/5 mM DTT/1 mM EDTA, pH 9, at 4°C. Followed by buffer exchange to 50 mM Tris/1 mM EDTA, pH 7.0, additional purification was performed using glutathione Sepharose.

Biochemical characterization of protein fibrillation. Kinetics of protein fibrillation was monitored by thioflavin T fluorescence using SpectraMax M2 (Molecular Devices). In a 96-well plate, 150 μl of the sample solution containing 5 μM proteins in 100 mM Na-Pi/100 mM NaCl/16.7 μM thioflavin T, pH 8.0, were set per well. A fibrillation reaction starts by adding 2 U of a HRV3C protease (Novagen), which specifically cleaves the site between GST and Htt42Q/TIA-1^{C}. A fluorescence signal was monitored at 20°C at intervals of 2 min with 442 and 485 nm of excitation and emission wavelength, respectively. The plate was shaken for 5 s before each fluorescence reading. For a seeding reaction, no plate shaking was performed before each measurement.

Protein aggregation was also examined in a 96-well plate using a Bio-Shaker MBR-024 (TAITEC). One-hundred fifty microliters of 10 μM proteins in 100 mM Na-Pi/100 mM NaCl/1 mM EDTA/5 mM TCEP, pH 7.0, were set per well, which was shaken overnight at 1200 rpm, 37°C. For a measurement of thioflavin T fluorescence, 10 μl of the sample solution was mixed with 90 μl of 100 mM Na-Pi/100 mM NaCl/1 mM EDTA/25 μM thioflavin T, pH 7.0. A fluorescence signal was obtained using a plate reader, ARVO MX (PerkinElmer), with a CW-lamp filter (440 nm cutoff) and an emission filter (486 nm cutoff). For a Congo red binding assay, a sample solution (150 μl; 10 μM) was first ultracentrifuged (TLA55; Beckman Coulter) at 50,000 rpm for 30 min at 4°C, and the protein precipitate was then resuspended in 50 μl of 100 mM Na-Pi/100 mM NaCl/1 mM EDTA, pH 7.0. Ten microliters of the resuspended solution was mixed with 90 μl of 100 mM Na-Pi/100 mM NaCl/1 mM EDTA/5 μM Congo red, pH 7.0, and electronic absorption spectra were recorded using Shimadzu UV-2400PC.

To observe aggregate morphologies using an electron microscope, protein aggregates were first adsorbed on 400-mesh grids coated by a glow-charged supporting membrane. For an immunoelectron microscopic observation, the aggregates adsorbed on the grids were further incubated with mouse monoclonal anti-Htt (EM48; Millipore Bioscience Research Reagents) and rabbit polyclonal anti-hemagglutinin (HA) (Y-11; Santa Cruz Biotechnology) antibodies in 1:250 dilution. After being washed with 0.1 M phosphate buffer, the aggregates were then incubated with colloidal gold-conjugated secondary antibodies (anti-mouse with 5 nm gold particle and anti-rabbit with 10 nm gold particle; British Biocell) in 1:250 dilution. After washing with 0.1 M phosphate buffer and pure water, negative staining with neutralized 2% sodium phosphotungstic acid was performed. Images were obtained using an electron microscope (1200EX; JEOL).

Images of atomic force microscopy were acquired on a Digital Instruments Multimode Nanoscope IIIa scanning microscope using a J-Scanner. Solution containing TIA-1^{C} aggregates (10 μl) were deposited on freshly cleaved mica substrate and incubated for 1 min. Unbound proteins and salt in the buffer solution were washed away with 50 μl of H_2O. Imaging was performed in tapping mode with RTESP (Veeco) cantilevers and acquired at a scan rate of 1.0 Hz with 512 lines per image.

Transgenic mice. The mouse experiments were approved by the animal experiment committee of the RIKEN Brain Science Institute. Details of transgenic mice, R6/2, have been published previously (Davies et al., 1997). Brain homogenates were fractionated as previously described (Díaz-Hernández et al., 2004), and an outline of the fractionation is also shown in Figure 1 *D*. Slight modifications of the fractionation were performed as follows; after treatment with 1% Sarkosyl in PBS containing 1% β-mercaptoethanol, the pellet was washed with 4% Sarkosyl in PBS. Additional wash of the pellet was done with 2% SDS in PBS. The pellet was then dissolved by incubation in 100% formic acid at 37°C for 1 h, dried up using SpeedVac, and redissolved in PBS containing 2% SDS. Protein concentration was determined by a BCA assay using BSA as a standard.

Plasmid construction for cell transfection. All plasmids including TIA-1 variants, Htt60Q-green fluorescent protein (GFP), Htt18Q-yellow fluorescent protein (YFP), Htt62Q-YFP, Htt62Q-cyan fluorescent protein (CFP), and Htt150Q-CFP were constructed using either pIRESneo3 (Clontech) or pcDNA3.1 (Invitrogen). YFP used in this study is an improved version of YFP called Venus (Nagai et al., 2002). In some experiments, coexpression of Htt18Q/62Q-YFP and TIA-1^{FL}-HA was performed by using a modified pIRESneo3 vector (pIRES-TIA-1), in which a neomycin phosphotransferase coding sequence (*SmaI*/*XbaI*) is replaced with TIA-1^{FL}-HA, and Htt18Q/62Q-YFP was inserted in the multiple cloning site (*AgeI*/*Bam*HI) of pIRES-TIA-1.

A pre-micro-RNA (miRNA) sequence targeting a human TIA-1 gene was cloned into a pcDNA6.2-GW/EmGFP-miR vector (Invitrogen). A forward sequence is as follows: 5′-TGCTGATGTGCTGCACTTTCATGGGAGTTTTGGCCACTGACTGACTCCCATGAGTGCAGCACAT-3′. An miR-LacZ provided by Invitrogen was used as a negative control for miRNA experiments.

Cell culture and sample preparations. Neuro2a cells as well as HEK293T cells were maintained in DMEM containing 10% FBS and penicillin/streptomycin and transfected with plasmid(s) indicated in each experiment using Lipofectamine 2000 (Invitrogen) according to the manufacturer's instructions.

For preparation of Htt/TIA-1 coaggregates formed in cells, *Neuro2a* cells in a six-well plate were transfected per well with 2 μg of pIRESneo3 containing Htt62Q-YFP together with 2 μg of pIRESneo3 containing either TIA-1^{FL}-HA or TIA-1^{C}-HA. After 4 h of transfection, a medium was changed to DMEM containing 10% FBS and 5 mM N^6,2′-*O*-dibutyryl cAMP (dbcAMP) (Nacalai Tesque). The cells were further incubated for a day and then lysed with 2% SDS in PBS with a Complete protease inhibitor mixture (Roche), sonicated, and ultracentrifuged with 50,000 rpm for 30 min at 4°C (TLA55; Beckman Coulter). Pellets were washed once with 2% SDS/PBS and twice with PBS. After being resuspended in PBS, the pellets were immunodecorated by anti-Htt and anti-HA antibodies with gold-conjugated secondary antibodies (5 and 10 nm, respectively) and observed by an electron microscope.

For functional analysis of TIA-1 in a cell, HEK293T cells in a six-well plate were transfected with 2 μg of pIRESneo3 or pIRES-TIA-1 containing Htt18/62Q-YFP cDNA and 2 μg of pPUR (Clontech). After 24 h of transfection, 1.5 μg/ml puromycin was added.

TIA-1 knockdown experiments were performed by transfecting HEK293T cells with 4 μg of pcDNA6.2-GW/EmGFP-miR containing miR-LacZ (negative control) or miR-TIA-1. After 24 h transfection, 10 μg/ml blasticidin was added.

In the functional analysis of TIA-1 as well as TIA-1 knockdown experiments, the cells were further incubated for 2 d after addition of antibiotics and then lysed in 150 μl of a radioimmunoprecipitation assay (RIPA) buffer containing a Complete protease inhibitor mixture with sonication. After ultracentrifugation (TLA55; Beckman Coulter) at 50,000 rpm for 30 min at 4°C, a supernatant was saved as a RIPA-soluble fraction. The pellet was washed once with a RIPA buffer, sonicated, and incubated in 100 μl of formic acid at 37°C for 1 h. After being dried up